This is a preprint, the final version is subject to change, of the American Mineralogist (MSA)
Cite as Authors (Year) Title. American Mineralogist, in press.
(DOI will not work until issue is live.) DOI: http://dx.doi.org/10.2138/am.2014.4683

Revision 1

Effects of chemical composition and temperature on transport properties of silica-rich glasses and melts

Anne M. Hofmeister[1,*], Alan G. Whittington[2], Jonas Goldsand[1], and Reinhardt G. Criss[3]

[1] Department of Earth and Planetary Sciences, Washington University, St. Louis, MO, 63130 USA

[2] Department of Geological Sciences, University of Missouri, Columbia, MO 65201, USA

[3] Horton-Watkins High School, Ladue MO, 63124 USA. Now at Case Western Reserve University, Cleveland OH 44106

*Corresponding author Hofmeist@wustl.edu 314-935-7440, fax 935-7361

Version 9/23/13 For American Mineralogist

Word count = ~8800 + 9 figures + 8 tables; Abstract = 251 words

Abstract

Combining new measurements of thermal diffusivity (D) and viscosity (η) of 13 silica-rich glasses and their melts with previous data reveals specific effects of Al, Ca, and Fe cations on heat and mass transport for diverse glasses and melts. We investigated rhyolites, tektites, leucogranite, haplogranite, and chemically complex commercial glasses. Highly polymerized samples, with high Al but low Ca contents, yield high values for η, D, and glass transition temperatures ($T_{g,12}$), whereas less polymerized samples with high Ca but low Al contents, have

low η, D, and $T_{g,12}$. Upon crossing the glass transition, D decreases substantially, to ~0.35 mm^2s^{-1} for Ca-rich melts, but D decreases only weakly, to ~0.52 mm^2s^{-1} for Al-rich melts. The magnitude of the decrease in D at $T_{g,12}$ correlates with the melt fragility, and also to the configurational heat capacity. High Ca contents result in low D for glasses and melts, whether or not Al is present. At high T, $\partial D/\partial T$ is positive for glasses and melts containing Fe^{2+}, which we attribute to diffusive radiative transfer involving electronic-vibronic coupling. Thermal conductivity of all glasses increases with T, flattening out as the transition is approached. For melts with ≥1 wt.% FeO_{total}, $\partial k/\partial T$ is positive. We predict that upon melting, I-type arc granite liquids should have lower thermal diffusivity than calcium-poor A- or S-types, and calc-alkaline basalts will have lower D than tholeiitic basalts, such that D of granitic melts is ~0.2 mm^2s^{-2} higher than basaltic. Ferrous iron enhancing heat transport could alter the predicted order at higher temperatures.

Keywords, laser-flash analysis, high-temperature, thermal diffusivity, viscosity, hydration, impurities, glass, melt

INTRODUCTION

Transport properties of rocks and magmas strongly influence igneous processes (e.g., Nabelek et al. 2012). Mass transport of a melt is described by viscosity (η), for which several predictive models exist as functions of temperature and composition (e.g., Hui and Zhang 2007; Giordano et al. 2008). Heat transport is described by thermal conductivity (k). Direct measurements of k of melt using contact methods are not reliable, because at the high temperatures (T) required, ballistic radiative transfer gains, exceed the lattice contribution (e.g., Hofmeister et al. 2007; 2009). Ballistic (direct or boundary-to-boundary) radiative transfer,

which goes roughly as T^3, is not a material property and is due to light passing essentially unattenuated through the sample. This ballistic radiative transfer does not occur in geological settings, but over the small length-scales encountered in the the laboratory it occurs at all temperatures, even cryogenic (e.g., Hofmeister, 2010; Hofmeister and Whittington 2012).

Thermal diffusivity (D) can be measured a few hundred K above the glass transition using laser-flash analysis (LFA), thereby providing information on the liquid state. The contact-free LFA technique (Parker et al. 1961) lacks systematic errors associated with conventional methods, such as thermal losses at interfaces of ~10% per contact. Furthermore, ballistic radiative transfer gains are removed after Diegiovanni et al. (1994) and Mehling et al. (1998), making the LFA technique essential for measuring thermally insulating, but highly transparent, glasses and melts with a high degree of accuracy (±2%). Combining our data with heat capacity (C_P) and density (ρ) data, which are generally available or can be estimated with reasonable accuracy (e.g. Richet 1987; Lange 1997), therefore constrains thermal conductivity (k) associated with vibrational modes, needed for thermal models of igneous processes,

$$k_{\text{lat}} = \rho C_P D. \quad (1)$$

Previously, we focused on simple glass compositions corresponding to the stoichiometry of crustal minerals, quartz (SiO_2); alkali feldspar ($XAlSi_3O_8$ where X = Li, K, Na), anorthite ($CaAl_2Si_2O_8$), and clinopyroxene ($XYSi_2O_6$ where XY = CaMg, LiAl, NaAl) (Pertermann et al. 2008; Hofmeister et al. 2009; Hofmeister and Whittington 2012). Studying natural rhyolites (Romine et al. 2012) showed that minor amounts of crystals significantly increase thermal diffusivity, due to their D-values being much larger than D of the glass matrix. In the absence of microcrystals, mass and heat transport properties are linked to chemical composition such that a

dichotomy exists between properties of mafic and felsic liquids, with the latter having higher viscosity and higher thermal diffusivity (Hofmeister et al. 2009).

To probe the effects of specific cations on thermal diffusivity, and to test whether the observed correlation of mass and heat transport properties holds for all high-silica chemical compositions, we examined diverse types of samples: natural glasses, laboratory synthetics and various commercial glasses, antique and modern. The 13 glasses selected have high silica contents (71-80 wt.% SiO_2), but variable quantities of other cations (Al_2O_3, FeO, MgO, CaO, Na_2O, K_2O). We present *D* vs. *T* for four highly polymerized Al-rich samples and five less polymerized Na- and Ca-rich samples, and compare these data to results for chemically similar remelted rhyolites of Romine et al. (2012), which lack crystallites. Our results above the glass transition provide reliable temperature derivatives for *D* of silicate melts, and further suggest that lattice thermal heat transport involves a form of radiative transport in the infrared, in addition to phonon scattering. We also include viscosity measurements of the molten state for compositions not heretofore investigated, which substantiate our previous demonstration that mass and heat transport properties are linked, and confirm that a dichotomy exists between transport properties of felsic and mafic melts. The new results imply differences in transport properties between granitic melts of different chemical types, and by extension also for basaltic melts of different types.

EXPERIMENTAL METHODS

88

89 **Sample compositions and synthesis procedures**

90 Our samples fall into two groups. One group includes two tektites, remelted leucogranite
91 and rhyolites, and a synthetic haplogranite, which all have high Al contents and low abundances
92 of other cations. The other group consists of antique and modern commercial glasses with high
93 Na and Ca, but low Al contents. Antiques are typically bubbly and often inhomogeneous due to
94 starting materials being more variable and manufacturing processes being less controlled. Within
95 each of these groups lesser variations exist in other cations, e.g., Fe, Mg and K (Table 1).
96 Moldavite is especially SiO_2-rich (>80 wt.%) whereas indochinite contains 5 wt % total
97 FeO. Remelted leucogranite from Harney Peak in the Black Hills, SD is described by
98 Whittington et al. (2009a). For obsidian from Mono Craters, California see Romine et al. (2012).
99 One of the rhyolite remelts was contaminated by the alumina crucible, providing a composition
100 with an Al/Si ratio like that of indochinite, but with low Fe. We also prepared a synthetic
101 haplogranite (corresponding to the 2 kbar H_2O-saturated minimum melt composition in the
102 $NaAlSi_3O_8$-$KAlSi_3O_8$-SiO_2 ternary system) by grinding appropriate combinations of SiO_2,
103 Al_2O_3, Na_2CO_3 and K_2CO_3 powders under acetone, then heating slowly in a platinum crucible to
104 1650˚C, driving off CO_2. Mass losses were consistent with full decarbonation. The liquid was
105 quenched to glass by cooling in air, then ground under acetone, and fused again. A third fusion
106 over 72 hours at 1650˚C allowed air bubbles to escape and ensured homogeneity.

107

108 **Sample preparation**

109 For parallel plate viscometry, cylindrical samples were cored from glass lumps using a
110 diamond core drill, avoiding visible bubbles. The cylinders were cut to lengths of 5 to 10 mm

111 using a diamond wafer saw, polished on successively finer grit papers, and parallel faces were
112 verified using a micrometer. For LFA, sections were sawed and ground into disks of ~12 mm
113 diameter with 0.5 to 1.1 mm thicknesses and nearly parallel surfaces, and sand-blasted with 50–
114 150 μm alumina grit. For spectroscopic measurements, double-polished sections were prepared.
115 Polished chips were used in electron microprobe analysis.
116
117 **Chemical analyses**
118 Samples were characterized by wavelength dispersive analysis (WDS) and standard
119 procedures on the JEOL-733 and JXA-8200 electron microprobes at Washington University,
120 using "Probe for Windows" for data reduction (see http,//www.probesoftware.com/). The
121 measured data were corrected with CITZAF after Armstrong (1995). Oxide and silicate
122 standards were used for calibration (e.g., Amelia albite for Na, Si; microcline for K; Gates
123 wollastonite for Ca; Alaska Anorthite for Al; synthetic fayalite for Fe; synthetic forsterite for
124 Mg; synthetic TiO_2 for Ti; synthetic Mn-olivine for Mn; synthetic Cr_2O_3 for Cr).
125
126 **Near-IR to ultraviolet spectroscopy and analysis of water contents**
127 Our evacuated Bomem DA3.02 Fourier transform interferometer has an SiC source, a
128 InSb detector, a CaF_2 beamsplitter. About 2000 scans were collected at room temperature from
129 ~1800 to ~9000 cm^{-1} at a resolution of 2 cm^{-1}. Unpolarized spectra from 9090 to 52630 cm^{-1} were
130 collected using a double-beam Shimaduzu UV-1800 with 1 nm resolution. Absorption
131 coefficients (A) were calculated from thickness (L) measured using a digital micrometer from,
132 $$AL = -\log(I_{trans}/I_0). \quad (2)$$
133 Water content of glass was determined from,

$$H_2O \text{ wt \%} = 1802\, a/(\rho\varepsilon L), \quad (3)$$

where ρ has units of gL^{-1} (see Table 2) and thickness L has units of cm. We used ε = 75 L $mol^{-1}cm^{-2}$ for the ~3500 cm^{-1} peak from Okumura et al. (2003) because their rhyolite compositions are similar to our Al-rich samples. Uncertainties are ~5%, mainly from that of ε. We report the total water content as ppm OH^-, because water is expected to be dissolved mostly as hydroxyl at the low concentrations observed (Stolper 1982), although small amounts of H_2O molecules may be present.

For Na-Ca glasses, ε = 42 L $mol^{-1}cm^{-2}$ is accepted for the high-ν peak (Shelby, 2005). We used this value in Eq. 3 for the additional O-H stretch near 2900 cm^{-1} (Fig. 1) and summed the results. Relative concentrations are accurate, but absolute concentrations could vary by ~30% for the Na-Ca glasses, due to ε being estimated for the low-ν peak (Table 2). However, given that hydroxyl only lowers D by 0.006 mm^2s^{-1} per wt % H_2O (Hofmeister et al., 2006) and that these samples have so little water that an effect on D-values would be difficult to ascertain, we did not attempt to verify water contents by another method.

Density determinations

Glass density was obtained before and after viscosity measurements using the Archimedean method, with ethanol as the immersion liquid. Repeat measurements indicate precision is ± 2 kg m^{-3}. A small initial bubble fraction (<0.2 volume %) present in some samples should not significantly impact viscosity measurements.

154

155 **Viscosity measurements**

156 Viscosity was measured using a Theta Instruments Rheotronic III parallel plate
157 viscometer, with a constant uniaxial load of 1500 g, and a maximum temperature of 1000˚C.
158 Viscosity is calculated from the measured longitudinal strain rate, known load and calculated
159 instantaneous surface area, assuming perfect slip between sample and plates. Relatively low
160 finite strains were used (≤ 20%); samples remained cylindrical after measurement. Temperatures
161 in this study ranged from 520 to 988˚C; viscosity ranged from 3.1×10^{8} to 7.9×10^{13} Pa s. The
162 accuracy and precision of the measurements are ±0.06 log units, confirmed by repeat
163 measurements on multiple cores. For experimental protocol and instrument calibration see
164 Whittington et al. (2009b). For the rhyolites, viscosity was also measured at superliquidus
165 conditions using a Theta Instruments Rheotronic II 1600C Rotating Viscometer, equipped with a
166 Brookfield HBDV-III Ultra measuring head, which can measure over the range 1 to 10^{5} Pa s
167 with accuracy and precision of ±0.03 log units, based on repeat measurements of NIST standard
168 glasses. For experimental protocols and calibration see Getson and Whittington (2007).

169

170 **Thermal diffusivity measurements**

171 Our LFA 427 apparatus is manufactured by Netzsch Gerätebau, Germany. Specimens are
172 held in a furnace in an Ar gas atmosphere using graphite holders. The temperature dependence of
173 *D* is obtained by varying furnace temperature, which is measured to within ~1˚C using calibrated
174 W-Re thermocouples. A pulse with ~ 0.5 ms width from a 400 W Nd-GGG laser heats the
175 sample from below, providing a difference of ~<4˚C across the sample. As heat diffuses from the
176 bottom to the top of the sample, emissions upward are recorded as a function of time with an

177 InSb detector. Graphite coatings on the sample serve to block laser light, enhance absorption of
178 the laser pulse and sample emissions, and buffer oxygen fugacity at high temperatures to C-CO.
179 Some samples (as noted) were sputter coated with Pt prior to graphite coating, to further block
180 unwanted direct (ballistic) light transfer through the sample. Data were obtained at 50-100 °C
181 intervals with several acquisitions at each temperature, and processed using the algorithm of
182 Mehling et al. (1998) to extract thermal diffusivity from the time-dependent emissions. This
183 model accounts for radiative surface losses to the surroundings and spurious radiative transfer
184 through the sample between the top and bottom graphite coats, and allows for absorbance being
185 frequency dependent, although the detailed values of optical properties are not needed. The
186 measured shape of the laser pulse is accounted for (Blumm and Opfermann 2002). Thermal
187 diffusivity is accurate to 2%, verified against opaque reference materials.
188
189 **CHEMICAL COMPOSITIONS, FE SPECIATION, AND WATER CONTENTS**
190
191 All investigated samples have high silica contents, spanning the range 71-80 wt % (Table
192 2). Granitic glasses and tektites have high Al_2O_3 (10-14 wt %) and moderate K_2O (2.5-4.6 wt %)
193 whereas commercial glasses have high CaO (7-14 wt %) and high Na_2O (12-16 wt %). A few
194 other cations are significant, the "1960" and modern Na-Ca glasses contain moderate MgO (up
195 to 4.6 wt%), and the indochinite contains 4.8 wt % FeO. Laboratory synthetics inherited some
196 trace impurities from the starting materials. The chemical composition of our moldavite is
197 consistent with that of 93 samples from the main strewn field (Bouška 1998) and with those from
198 the stated location (Philpotts and Pinson 1966). Our indochinite is most similar to the normal

australites, but has slightly lower Ca, Na and Mg. This difference is insignificant because few samples were previously analyzed (Chapman and Scheiber 1969; Koberl 1986).

To make comparisons with our previously examined samples with feldspathic stoichiometry, Table 1 provides "formulae" based on eight O atoms. Polymerization is often quantified by the nominal ratio of non-bridging oxygens to tetrahedrally-coordinated cations (NBO/T). In Table 2, NBO/T is calculated assuming that all Si, Ti, Al and Cr are network-forming tetrahedral cations and all other cations either play a charge-balancing role for tetrahedral Al and Cr, or are network-modifying cations that result in some non-bridging oxygens. Although unlikely to be strictly correct, these assumptions provide a useful first-order assessment of the state of polymerization of the glass structures. For most samples, Fe contents are low and are unimportant to our evaluation. The tektites and leucogranites with high Fe mostly have Fe^{2+} (see spectra below) and thus are represented correctly in our NBO/T calculation. Antique glasses have high NBO/T values in the range 0.63-0.79, which are more typically associated with basalts and mafic melts, whereas Al-rich granites and rhyolites have low NBO/T below 0.02, and the tektites have NBO/T = 0.07.

Infrared spectra for high Al glasses prior to heating have a broad, asymmetric band near 3550 cm^{-1} (e.g. indochinite, Fig. 1), as do rhyolites of Okamura et al. (2003), whose calibration we used to quantify hydration. The profile indicates hydroxyl (OH^-). Water contents are low and decreased upon heating during LFA (Table 2). Water contents of our impact melts agree with previous determinations of 70 -130 ppm for moldavites (Luft 1983) and of 20-190 ppm H_2O in indochinites and australites (Gilchrist et al. 1969). Water contents are too low to observe overtone-combination bands at higher frequency (Fig. 2a).

Low Al (high Ca) glasses have a second broad peak near 2900 cm^{-1} (e.g., 1926, Fig. 1). The position indicates hydrogen bonding associated with nearby O^{2-} atoms (e.g., Rossman 1988a). If scattering baselines are accounted for, the two peaks decrease together with heating. Because hydroxyl contents of the glasses are similarly low, trends in thermal diffusivity are attributed to variations in cations other than H.

Visible spectra (Fig. 2) show d-d electronic transitions of iron, assigned by comparison to mineral spectra of Rossman (1988b). Bands for octahedrally coordinated Fe^{2+} are present at >0.1 wt % FeO, and in the antiques with lower FeO contents, but not in modern glass or haplogranite, which have much weaker UV tails, consistent with the absence of Fe^{2+} that interacts with existing Fe^{3+} (as observed for orthopyroxenes, Hofmeister 2012). The position of the main Fe^{2+} band shifts from 8930 cm^{-1} in the Al-rich glasses to 10000 cm^{-1} in the Na-Ca glasses. Sharp bands for tetrahedrally coordinated Fe^{3+} occur at 22833, 23780, and 26260 cm^{-1} for Na-Ca glasses, and at slightly higher positions for haplogranite. For leucogranite and rhyolite with higher FeO (1.0 wt %), these Fe^{3+} transitions are at similar positions but are broader. We conclude that Fe^{3+} bands in both tektites are too broad to be resolved as shoulders on their strong UV tail. For the four Al-rich glasses with >1 wt % FeO, an additional broad band exists near 18460 cm^{-1}. We assign this to intervalence charge transfer (IVCT) due to its spectral profile and position, and evidence for both charge states of Fe. In the moldavite the broad band is not resolvable but is the cause of high absorbance in the visible (Fig. 2). Indochinite spectra are like moldavite, but more intense (not shown). To locally balance charge, Fe^{3+} is likely preferentially located adjacent to Fe^{2+}. This conclusion is supported by comparing the strength of the Fe^{2+} absorption in Fig. 2a to the total FeO content. Relative band strengths for 1895 and leucogranite are proportional to their FeO contents, but the band for moldavite is ~50% stronger and that of

indochinite is ~100% stronger, compared to low Fe glasses. Band enhancement connected with IVCT is well-known (Rossman 1988b). Rhyolite spectra are similar to the leucogranite, but have slightly stronger IVCT, attributed to specific site locations. Similarly, disproportionately large band strengths for Fe^{3+} in 1960 compared to the other low Fe glasses are attributed to interactions without charge transfer, as observed in minerals (e.g., Rossman 1988b).

RESULTS ON TRANSPORT PROPERTIES

Viscosity

Near the glass transition, viscosity is close to a linear function of inverse temperature for all samples, although the antique liquids have lower viscosity and steeper slopes than the tektites and granites (Fig. 3; Table 3). Both viscosity and the viscometric glass transition temperature, taken to be the temperature of the 10^{12} Pa s isokom ($T_{g,12}$), decrease with decreasing melt polymerization from granites to tektites to antiques (Table 4). A decrease in $T_{g,12}$, and in viscosity at any given temperature, accompanies increasing Al/Si ratio from haplogranite to leucogranite, and from moldavite to indochinite, whereas decreasing $T_{g,12}$ correlates with increasing Na/Ca in the commercial specimens.

Datasets were fitted with the Tamman-Vogel-Fulcher (TVF) equation,

$$\log \eta = A + B/(T\text{-}C) \quad (4)$$

where A, B and C are adjustable parameters. Best-fit values are given in Table 4. It is generally accepted that all silicate melts tend towards a common value of about $10^{-4.5}$ Pa s at very high temperatures (Russell et al. 2003), so the antique liquids, which have a relatively low glass transition temperature but also a steep slope on Figure 3, must show pronounced non-Arrhenian

267 behavior at higher temperatures than investigated here. Although the best fits for many of our
268 samples return an A value in the range -4 to -5, we did not force all the fits to a common value.
269 Given the large number of viscosity data for each sample, all three TVF parameters are tightly
270 constrained, allowing extrapolation of viscosity with a high degree of confidence up to the
271 highest temperatures at which samples were analyzed by LFA, which is useful in interpreting
272 changes in *D* observed at high temperatures.

273 One way to quantify the degree of non-Arrhenian behavior, or "fragility", is to calculate
274 the gradient of the viscosity curve at the glass transition temperature on a reduced temperature
275 scale (Plazek and Ngai 1991); see Table 4. Melt fragility is directly related to configurational
276 heat capacity, C_P^{conf}, which is the difference between C_P of the glass at T_{12} and of the melt
277 (Richet et al. 1986). From the temperature dependence of relaxation times in viscous liquids
278 (Adam and Gibbs 1965), the viscosity of a liquid can be related to its configurational entropy
279 (S^{conf}) through,

280 $$\log \eta = A_e + \frac{B_e}{TS^{conf}(T)} \qquad (5)$$

281 where T is temperature, A_e is a constant, and B_e is another constant reflecting the Gibbs free-
282 energy barriers hindering co-operative rearrangements in the liquid (Richet 1984). Highly
283 polymerized melts with small values of C_P^{conf} have small changes in S^{conf} with temperature, and
284 hence exhibit near-Arrhenian or "strong" behavior (Richet and Bottinga 1995). Conversely, less
285 polymerized melts with large values of C_P^{conf} have correspondingly large changes in S^{conf} with
286 temperature, and hence exhibit distinctly fragile, non-Arrhenian, behavior. Calculated values of
287 fragility for our samples show the expected positive correlation with NBO/T (Table 4), such that
288 granites (NBO/T = 0) are the least fragile, the tektites (NBO/T = 0.07) are intermediate, and the
289 Ca-rich compositions (NBO/T = 0.63 to 0.79) are the most fragile.

290

291 **Thermal diffusivity**

292 Thermal diffusivity of glasses is highest at room temperature, decreases with increasing
293 temperature, and becomes nearly constant at high T (Fig. 4), as observed for other silicates (e.g.,
294 Hofmeister et al. 2009). Greater variability is associated with the antiques (Fig. 5ab), attributed
295 to inhomogeneities such as the presence of tiny bubbles, and variations in fictive temperature and
296 internal strain induced by different annealing and/or quenching rates (see notes in Table 1). For
297 samples with high Al and Fe^{2+} contents, which remained glass to high T, $\partial D/\partial T$ is slightly
298 positive above 800 K (Figs. 4 and 5cd), similar to the behavior of SiO_2 glass from ~1000 K up to
299 the glass transition (Hofmeister and Whittington 2012).

300 As in our previous studies, D decreases substantially across the glass transition (Fig. 5).
301 Our measurements probe relaxed melt, starting at T corresponding to a viscosity of $\sim 2\times10^8$ Pa s
302 (e.g., Pertermann et al. 2008; Hofmeister et al. 2009). The temperature of the transition in LFA
303 being higher than in viscometric experiments can be understood by considering the relaxation
304 timescale (τ) calculated from the Maxwell relationship ($\eta = G_\infty\tau$) where G_∞ ~10 GPa, see
305 Dingwell and Webb 1990 and Whittington et al. 2012) is ~1–10 ms, consistent with the duration
306 of the laser pulse in LFA. Glass transition temperatures in our heat transfer experiments ($T_{g,LFA}$)
307 occur at substantially higher temperatures and lower viscosities than in viscometry experiments
308 ($T_{g,12}$) simply due to the short timescale on which the laser interrogates the sample. At moderate
309 T only a little above $T_{g,12}$, viscous liquid appears frozen (glassy) on the short timescale of the
310 laser pulse, although it can still flow over the longer (minutes to hours) timescale of a viscosity
311 measurement. Although the state immediately above the glass transition is supercooled
312 (metastable) liquid, thermal diffusivity measured above $T_{g,LFA}$ represents that of structurally

313 relaxed melt up to and including superliquidus conditions, and is denoted D_{melt}. For brevity, we
314 refer to this state as liquid.

315 The glass-to-liquid transition occurred at very low temperatures for the Na-Ca specimens
316 (Fig. 4). The melt was initially viscous and flowed slowly, permitting acquisition of *D* of
317 supercooled liquid over intervals of up to 300 K for some compositions (Fig. 5b) compared to
318 narrower ranges of <200 K previously. Because flow near 1200 K for the Na-Ca liquids is
319 accompanied by thickening and sagging, followed by thinning, as well as by loss of the small
320 amounts of water in the samples, the highest temperature points may not provide reliable
321 measurements. As discussed by Hofmeister and Whittington (2012), LFA samples are thin and
322 suspended by their edges so flow occurs below the sagging temperature, which is derived from
323 flow of lumps. Examining the recovered sample allowed us to estimate whether flow was
324 extensive, moderate, or slight, and to provide a similar assessment regarding the growth of
325 bubbles. Table 6 excludes suspect *D* values, such as 1926-1 (see below). Constant D_{melt} was
326 observed for the Na-Ca samples, which become liquid at relatively low temperatures, whereas
327 upturns (quantified below) exist for Al-rich samples for which higher temperatures were reached
328 (see Fig. 4). When degassing occurs, it is evident as bubbles appearing in the recovered samples
329 and reduction of O-H peaks in the IR spectra (Fig. 1, Table 2). Because the presence of OH^-
330 lowers the glass transition temperature, upon degassing, the material can return to the glass state
331 (*D* increases) and then become liquid once again as temperature increases: this behavior is
332 evident in only a few samples (Al-rich leucogranite and moldavite) and is marked by arrows in
333 Fig. 5cd. This process is not seen for Na-Ca samples which have stronger hydrogen bonding, as
334 indicated by lower O-H frequencies (Fig. 1) and thus require higher temperatures for
335 dehydration, at which point flow dominates over degassing. Note that the water contents (Table

336 2) are too small to measurably affect values of *D* (see Hofmeister et al., 2006), only the
337 temperature of the transition from glass to melt is affected by water loss.

338 Because variations in thermal history and internal strain strongly affected *D* of pure silica
339 glass (Hofmeister and Whittington, 2012), we performed multiple runs to different maximum
340 temperatures (T_{max}). High Na>Ca glass (the 1960 insulator) initially had a much steeper trend
341 than any other low Al glass, but above $T_{g,LFA}$, the temperature dependence of D_{melt} was like that
342 of the other commercial samples (Fig. 5a). Very little water was lost (Table 2), consistent with
343 the change in behavior being due to either removal of strain, or diffusion of the tiny bubbles. A
344 second disc of 1960 was run, but the cover had tilted so we do not show this suspect dataset. The
345 reruns of both discs of 1960 had low *D*-values (Fig. 5a), consistent with the presence of strain
346 developing as the sample sagged under its own weight but the trends resemble those of other
347 Na-Ca glasses and melts.

348 Rolled Na~Ca glass from 1926 has a wide range of initial values (Fig. 5b), which is likely
349 due to variable amounts of strain. However, *D* of liquid for disc #1 is much higher than for other
350 discs (#2-4), which are equal within uncertainty and resemble chemically similar vase and
351 modern liquids (Fig. 4). Melts are relaxed and thus strain cannot cause this difference. The
352 compositions are essentially the same (Table 2), so neither is chemistry the source. Hofmeister
353 and Whittington (2012) found that overly thick coats of Au on silica glass artificially elevated *D*
354 and also produced flatter trends than graphite coats. Because both features are observed for disc
355 #1 of 1926, which was Pt coated, we do not discuss the data for this disc further. Although
356 coatings of metals are desired for suppression of ballistic transfer, the very low *D*-values of
357 glasses being easily perturbed by coatings thicker than optimal, leads us to conclude that graphite
358 coatings alone are preferred.

Haplogranite had similar D for all three runs, as we observed for our previous laboratory synthetics (Perterman et al. 2008; Hofmeister et al. 2009). Slightly more variability was observed in the rhyolites, but these are the same within measurement uncertainty.

We considered several different formulae in fitting the T response for D of glass. The T^{-1} form expected for phonon scattering (e.g., Julian 1965) is obviously too steep for these flat lying trends. Instead, data for Na-Ca glasses could be fit to a simple power law, $T^{-0.1}$ to $T^{-0.4}$, but with low correlation coefficients (R~0.96, indicating a less than optimal fit). This behavior, coupled with observed upturns at high T for SiO_2 glass (Hofmeister and Whittington 2012) and Al-rich samples (Fig. 5cd) suggests one possible form,

$$D = a + bT^{-1} + cT. \quad (6)$$

With the additive constant, the linear cT term was not needed for the high Na-Ca glasses, but it significantly improved the fit for the Al-rich glasses (Table 5). Importantly, phonon scattering is not precisely inverse with T. Calculations for MgO, which has few IR modes, indicate a stronger inverse dependence, $\sim T^{-1.4}$ (e.g., de Koker 2010; Tang and Dong 2010), which is compatible with fits to LFA data on MgO (Yu and Hofmeister 2011). Hofmeister et al. (in prep.) found that LFA data on crystals are well-represented by

$$D = fT^{-g} + hT, \quad (7)$$

where g depends on crystal structure. For feldspar crystals with many IR modes, g = 0.3 to 0.85, such that g increases as Al-Si and Na-Ca ordering increases. For our glasses, which are highly disordered, we used g = 0.4, which describes the steep $\partial D/\partial T$ of sample 1960-1, and provided good fits (Table 5). Above $T_{g,LFA}$, we use a simpler fit, $D_{melt} = a + cT$.

DISCUSSION

382

383 **Comparison with previous measurements of heat transport properties**

384 Some contact-free measurements exist on melts with compositions similar, but not
385 identical, to ours, including Ca-Al-Si slags (Erikson and Seetharaman 2004) and Na-Ca-Si oxide
386 glasses used as standards in Japan (Shibata et al. 2005). The steep increase in D with T for all
387 slags of Erikson and Seetharaman (2004) is due to not accounting for the large amounts of
388 spurious radiative transfer which are present at high T (> 1600 K), and is discounted. Results of
389 Shibata et al. (2005) are roughly consistent with our data, given that the compositions differ
390 slightly . However, Shibata et al. (2005) used a non-standard geometry that does not permit
391 measuring heat crossing the sample, did not account for radiative transfer, and did not
392 benchmark their results, so accuracy is not yet established for their technique.

393 We do not compare our results to contact measurements of thermal conductivity because
394 techniques such as the hot wire method involve both contact losses of ~10% per contact and
395 radiative gains that can more than double intrinsic D (discussed by Hofmeister et al. 2007).

396

397 **Dependence of thermal diffusivity values on melt chemistry**

398 Figure 6 further shows that trends in D of liquid against cation contents are generally
399 similar to trends in D_{298} of glasses, although variations in D of the liquid are typically larger. The
400 average decrease in D from glass prior to the transition to relaxed melt is 0.15 mm^2s^{-1},
401 irrespective of temperature of the glass transition. Overall, the spread in D among different
402 melts is similar to the spread among glasses at room temperature. The consistency in Figure 6
403 indicates that we provide accurate values for D of melts above the glass transition, but before
404 significant flow or crystallization onsets.

We examined the variation of *D* as a function of the concentrations of various cations for both glasses and melts studied by LFA. The strongest correlations were found with Ca and Al content (Fig. 6), increasing concentrations of either cation lowers *D*. However, we recognize that multiple compositional effects coexist. For example, in Figure 6b, the three alkali feldspar compositions lack Ca and so their values depend on other factors, e.g., the size of the substituting cation. Importantly, high Ca contents clearly result in low values of thermal diffusivity whether or not Al is present (c.f. anorthite and diopside). This finding is consistent with the known large effect of Ca on thermal expansivity of melts (Fluegel et al. 2008) since *D* is connected with thermal expansivity for crystals and glasses (Hofmeister 2010; Hofmeister and Whittington 2012).

Our results suggest that high Ca content, and to a lesser extent high Al content, are the main chemical variables that reduce *D* in silicic melts. Therefore, Ca-rich magmas such as tonalities, trondhjemites, granodiorites, and I-type arc granites, are expected to have lower thermal diffusivity than similar, but calcium-poor rocks (A-type or S-type granites). At subliquidus conditions, the relatively high *D* of crystals compared to melt may become more important than variations in *D* caused by differences in melt chemistry. The crystallization history of the magma is itself a function of the thermal history, thus illustrating the potentially complex feedbacks between the two, mediated by magma transport properties.

Dependence of thermal diffusivity on structural properties

The decrease in *D* at T_g is consistent with configurational changes and similar behavior of C_P and D^{-1} (see Hofmeister et al. 2009; Hofmeister and Whittington 2012). Configurational changes in the liquid upon heating are approximated by the melt fragility. The nominal degree of

428 polymerization (NBO/T) is less useful because all feldspathic and haplogranitic melts are
429 nominally fully polymerized, yet they show a considerable range in *D*. Generally, both *D* of
430 glass and melt decrease as fragility increases (Fig. 7a). Other factors must also be important, as
431 indicated by divergence of silica and the Na-Ca glasses from the trend of our feldspar, pyroxene,
432 and various Al-bearing glasses. Nevertheless, this well-defined trend is pertinent to igneous melt
433 compositions, and provides further confirmation of the link between heat and mass transport
434 properties suggested by Hofmeister et al. (2009).

435 Density reflects both structural and chemical characteristics. The overall decrease in
436 D_{melt} as melt density increases (Fig. 7b) is attributed to increased phonon interactions, i.e. more
437 phonons in an equal volume of melt. Silicic melts typically have high *D* and η, and low fragility
438 and ρ, again linking heat and mass transport.

439

440 **Increase in *D* with *T for glass and liquid***

441 The initial decrease in thermal diffusivity with increasing temperature has long been
442 attributed to phonon scattering (Liebfried and Schlömann 1954; Julian 1965). At ~500 K,
443 increases in thermal diffusivity have been previously observed due to ballistic radiative transfer
444 between the heater and thermocouple, which do not actually involve the sample (see e.g.,
445 Hofmeister et al., 2007). In our LFA measurements, this unwanted ballistic radiative transfer has
446 been removed at all *T*. In the present study and in our study of SiO_2 glasses, we found that *D* of
447 the glass increases linearly with *T* above 1000 K, for samples that remained glassy at these high
448 temperatures (Fig. 5bc; also see Hofmeister and Whittington, 2012).

449 Our Fe- and Al-rich samples have obvious upturns and similar values for the linear
450 coefficient (Eqs. 6 and 7) for both glasses and their melts (Tables 5 and 6). Fitting suggests that

positive linear coefficients exist for the other samples, although slopes are poorly constrained for Na-Ca melts due to their low $T_{g,,LFA}$ and proclivity to flow at temperatures only a little higher (e.g. Figs. 4,5a). Given scatter in the data and uncertainties in fitting, the linear coefficients for glasses and melts are described approximately as, $<<10^{-5}$ K^{-1} for Na-Ca (glasses only) and haplogranite; 0.3-1 $\times$ 10^{-4} K^{-1} for leucogranite and the rhyolites, and 1.5-2 $\times$ 10^{-4} $K^{-1}$for the tektites. At higher temperatures, silica glass and melt both show positive $\partial D/\partial T$ of about 10^{-4} $mm^2s^{-1}K^{-1}$ (Fig. 5; Hofmeister and Whittington 2012). The present data show a strong correlation of the upturns with Fe^{2+} content and/or charge transfer between Fe^{2+} and Fe^{3+} (Fig. 2; Table 2).

It is possible that some of the increase in D observed in glasses at high temperature may be due to removal of defects by annealing, and for melts some of the increase could be due to flow of the sample within the experimental apparatus. However, this cannot be the case immediately above $T_{g,LFA}$ where the liquid is relaxed, yet still too viscous for flow to affect the measurements significantly.

It is unlikely that the increase in D with T is due to configurational entropy. Heat capacity and D^{-1} depend similarly on temperature (e.g., Hofmeister and Whittington 2012) so that across the glass transition, D drops whereas C_P increases. The magnitudes of the changes in D and C_P correlate (Fig. 12 in Hofmeister et al., 2009). The increase in D with T, if configurational, would mean that configurational heat capacity decreases with temperature, which is inconsistent with available data that suggest high temperature heat capacities of silicate liquids are constant or increase with temperature (see review by Mysen and Richet 2005, and references therein).

The positive correlation in the present study of the cT term in Equation 7 with Fe^{2+} is consistent with a radiative process, because the high frequency electronic transitions of Fe^{2+} are

coupled with vibronic transitions, as indicated by their extremely large bandwidths (cf. d-d transitions of Fe^{3+} to Fe^{2+} in Fig. 2). In intervalence charge transfer, electrons cross Fe^{2+}-O^{2-}-Fe^{3+} bonds, and thus lattice vibrations are involved. The present data suggest that reduction in heat transport due to cation disorder offset by the increase of D with T attributed to radiative effects.

Consequently, despite the decrease in D with increasing fragility, iron-rich tholeiitic melts may have relatively high thermal diffusivity values at high (liquidus) temperatures, especially compared to relatively iron-poor calc-alkaline basalts. Refining this speculation requires quantifying the linear term in Eqs. 6 and 7 and its dependence on Fe content for glasses and melts, and whether a similar enhancement exists for crystals, will require additional study.

THERMAL CONDUCTIVITY

Using Eq. 1 requires data on density and heat capacity. For C_P, we used the model of Stebbins et al. (1984) for liquid and that of Richet (1987) for glass. Rhyolite data are from Neuville et al. (1993). Density of soda lime melts are reproduced by the model of Fluegel et al. (2008) as a function of composition within a 95% confidence level, with a linear temperature-dependence (Table 7). Except for highest Ca sample (No. 1926), these results are close to the formulation of Lange (1997), which also yields density that depends linearly on T. Because the model of Fluegel et al. (2008) reproduces experimental data for industrial glasses and melts, and the effect of Ca is known to be large, we use the Lange (1997) model for the Al-rich melts, which have compositions similar to measurements underlying her model. For the Al-rich glasses, no data exists on $\rho(T)$. Given the calculated expansivity values for soda-lime silica glasses reported in Table 7, we use $\alpha_{glass} = 20\ \mu K^{-1}$ combined with measured room temperature density (Table 1). Changes in density are minor compared to changes in D and C_P as a function

497 of temperature, for crystals, glasses and melts. Note that the largest uncertainty in k is due to how
498 accurately C_P is modeled.. For this reason our report has centered on thermal diffusivity.
499 Thermal conductivity of glasses increases with T (Fig. 8) due to the strong increase of C_P
500 with temperature overwhelming the weak decreases of density and of thermal diffusivity (Figs. 4
501 and 5). Because k is the product of C_P and D, which respond oppositely to increasing
502 temperature, and the models of C_P have uncertainties, configurational effects on k are not easily
503 resolved, and we leave this issue for later studies. For the melts, thermal conductivity depends
504 linearly on T (Table 8) because all three inputs have this form. Whether $\partial k/\partial T$ is positive or
505 negative depends on the relative sizes of the input derivatives. For the Na-Ca glasses, C_P was
506 estimated as constant, whereas this property could increase slightly due to anharmonicity. If this
507 is indeed the case, then k of the Na-Ca melts is approximately temperature independent, and
508 equal to the value obtained at the transition. For the Al-rich melts, within uncertainty, the
509 positive $\partial k/\partial T$ trend obtained for the glass extrapolates into the melt field (Fig. 8b). These strong
510 melts have very small configurational heat capacities, so crossing the glass transition should
511 result in only modest changes in physical properties, as observed.
512
513 **IMPLICATIONS FOR GEOLOGIC MELTS**
514 This paper provides high T measurements of D that are free from experimental artifacts
515 such as ballistic radiative transfer gains and contact losses. Key findings are: (1) The cations Ca,
516 Al and Fe strongly affect values of heat and mass transport properties of silicate glasses and
517 melts, whereas substitution of Na and K have a minor effect. Polymerization has a strong effect,
518 as described by melt fragility, but both are overridden by the presence of Ca. The physical cause
519 for the decrease in D with Ca content is tentatively attributed to Ca vibrations being at low

520 frequency, which promote mode-mixing with acoustic phonons, which species largely control
521 phonon-phonon scattering (e.g., Tang and Dong, 2010) and to optical phonons being slower (less
522 efficient) than acoustic. (2) Thermal diffusivity of glass and melt can increase with T at high T,
523 and the magnitude of the increase is correlated with the presence of Fe. (3) Regular variations of
524 glass and melt properties with chemical composition previously discovered for simple glass
525 compositions also hold for more chemically complex glasses.

526 These inferences, along with the trends of D_{melt} with composition and physical properties,
527 permit estimation of thermal diffusivity near liquidus of melts associated with common igneous
528 and volcanic rocks (Fig. 9). Felsic melts with low Ca contents are expected to have high D_{melt}
529 ~0.5 mm^2s^{-1}. This projection includes most granite and granitoid melts, and involves little
530 uncertainty due to little variation in the end-member values. However, more calcic I-type arc
531 granite melts are expected to have lower thermal diffusivity than calcium-poor A-type or S-type
532 granites. Mafic melts will have low D_{melt} ~0.3 mm^2s^{-1}. This projection is less certain because of
533 D_{melt} of olivine was estimated and because the effect of Fe cations is strong, as shown in the
534 present paper. Consequently, we also predict that calc-alkaline basalts will initially have lower
535 thermal diffusivity than tholeiitic basalts. At high temperature the converse could hold due to the
536 higher Fe content of tholeiitic magmas.
537

538 **ACKNOWLEDGMENTS**

539 Support from NSF grants EAR-0748411, EAR-0911428, EAR-1321857 and EAR-0911116 is
540 appreciated. We thank Paul Carpenter (W.U.) for providing microprobe analysis.
541

542 **REFERENCES CITED**

543 Adam, G. and Gibbs, J.H. (1965) On the temperature dependence of relaxation phenomena in glass-
544 forming liquids. Journal of Chemical Physics, 43,139-146.
545 Armstrong, J.T. (1995) CITZAF, A package of correction programs for the quantitative electron
546 microbeam X-ray analysis of thick polished materials, thin films, and particles. Microbeam
547 Analysis, 4, 177-200.
548 Blumm, J. and Opfermann, J. (2002) Improvement of the mathematical modeling of flash
549 measurements. High Temperature High Pressure, 34, 515-521.
550 Bouska, V. (1998) The moldavite strewn field. Chemie der Erde, 58, 321-343.
551 Bouhifd, M.A., Whittington, A., and Richet. P. (2001) Partial molar volume of water in phonolitic
552 glasses and liquids. Contributions to Mineralogy and Petrology, 142, 235-243.
553 Burns, G. (1990), Solid State Physics. Academic Press, San Diego.
554 Chapman, D.R. and Scheiber, L.C. (1969) Chemical investigation of Australasian tektites. Journal of
555 Geophysical Research, 74, 6737-6776.
556 Degiovanni, A., Andre, S., and Maillet, D. (1994) Phonic conductivity measurement of a semi-
557 transparent material. In, Tong TW (ed) Thermal conductivity 22. Technomic, Lancaster, PA,
558 pp 623-633
559 de Koker, N. (2010), Thermal conductivity of MgO periclase at high pressure, implications
560 for the D″ region. Earth and Planetary Science Letters, 292, 392–398.
561 Dingwell, D.B. and Webb, S.L. (1990) Relaxation in silicate melts. European Journal of Mineralogy,
562 2, 427–449.
563 Erikson, R. and Seetharaman, S. (2004) Thermal diffusivity measurements of some synthetic
564 CaO-Al_2O_3-SiO_2 slags. Metallurgical and Materials Transactions, B35, 461-469.

565 Fluegel, A. (2007) Thermal expansion calculation of silicate glasses at 210°C, based on the
566 systematic analysis of global databases.
567 http,//glassproperties.com/expansion/Expansivity_Glass_2006.pdf. Accessed 7 September
568 2012
569 Fluegel, A., Earl, D.A., Varshneya, A.K., and Seward, T.P. III (2008) Density and thermal
570 expansion calculation of silicate glass melts from 1000°C to 1400°C. Physics and Chemistry
571 of Glasses, European Journal of Glass Science and Technology, B49, 245–257.
572 Gilchrist, J., Thorpe, A.N., and Senftle, F.E. (1969) Infrared Analysis of Water in Tektites and
573 Other Glasses. Journal of Geophysical Research, 74, 1475-1483.
574 Giordano, D., Russell, J.K., and Dingwell, D.B. (2008) Viscosity of magmatic liquids, a model.
575 Earth and Planetary Science Letters, 271, 123–134.
576 Hofmeister, A.M. (2010) Thermal diffusivity of perovskite-type compounds at elevated
577 temperature. Journal of Applied Physics, 107, locater number 103532
578 Hofmeister, A.M. (2012) Thermal diffusivity of orthopyroxenes at elevated temperature.
579 European Journal of Mineralogy, 24, 669-681.
580 Hofmeister, A.M. and Whittington, A.G. (2012) Effects of hydration, annealing, and melting on
581 heat transport properties of fused quartz and fused silica from laser-flash analysis. Journal of
582 Non-Crystalline Solids 358, 1072-1082.
583 Hofmeister, A.M., Pertermann, M., Branlund, J.M., and Whittington, A.G. (2006) Geophysical
584 implications of reduction in thermal conductivity due to hydration. Geophysical Research
585 Letters, doi,10.1029/2006GL026036

586 Hofmeister, A.M., Pertermann, M., and Branlund, J.M. (2007) Thermal Conductivity of the Earth.
587 In, Schubert G (ed). Treatise in Geophysics (Schubert G, Ed. In Chief) V. 2 Mineral Physics
588 (Price GD, ed.). Elsevier, The Netherlands, pp 543-578.
589 Hofmeister, A.M., Whittington, A.G., and Pertermann, M. (2009) Transport properties of high albite
590 crystals and near-endmember feldspar and pyroxene glasses and melts to high temperature.
591 Contributions to Mineralogy and Petrology, 158, 381-400.
592 Hui, H. and Zhang, Y. (2007) Toward a general viscosity equation for natural anhydrous and hydrous
593 silicate melts. Geochimica Cosmochimica Acta, 71, 403–416.
594 Jewell, J.M., Shaw, C.M., and Shelby, J.E. (1993) Effects of water content on aluminosilicate
595 glasses and the relation to strong/fragile liquid theory. Journal of Non-Crystalline Solids,
596 152, 32-41.
597 Julian, C.L. (1965) Theory of heat conduction in rare-gas crystals. Physical Review A, 137, 128-137.
598 Knoche, R., Dingwell, D.B., and Webb, S.L. (1992) Non-linear temperature dependence of
599 liquid volumes in the System albite-anorthite-diopside. Contributions to Mineralogy and
600 Petrology, 111, 61-73.
601 Knoche, R., Dingwell, D.B., and Webb, S.L. (1995) Melt densities for leucogranites and granitic
602 pegmatites, partial molar volumes for SiO_2, Al_2O_3, Na_2O, K_2O, Li_2O, Rb_2O, Cs_2O, MgO,
603 CaO, SrO, BaO, B_2O_3, P_2O_5, F_2O_{-1}, TiO_2, Nb_2O_5, Ta_2O_5, and WO. Geochimica
604 Cosmochimica Acta, 59, 4645-4652.
605 Koberl, C. (1986) Geochemistry of tektites and impact glasses. Annual Reviews of Earth and
606 Planetary Science, 14, 323-350.
607 Lange, R.A. (1996) Temperature independent thermal expansivities of sodium aluminosilicate
608 melts between 713 and 1835 K. Geochimica Cosmochimica Acta, 60, 4989-4996.

609 Lange, R.A. (1997) A revised model for the density and thermal expansivity of K_2O-Na_2O-CaO-
610 MgO-Al_2O_3-SiO_2 liquids from 700 to 1900 K, extension to crustal magmatic temperatures.
611 Contributions to Mineralogy and Petrology, 130, 1-11.
612 Lee, D.W. and Kingery, W.D. (1960) Radiation energy transfer and thermal conductivity of ceramic
613 oxides. Journal of the American Ceramic Society, 43, 594-607.
614 Liebfried, G. and Schlömann, E. (1954) Warmleitund in elektrische isolierenden Kristallen.
615 Nachrichten von der Gesellschaft der Wissenschaften zu Göettingen Mathematik und Physik
616 K1,71–93.
617 Luft, E. (1983) Zur Bildung der Moldavite beim Ries-Impakt aus Tertiären Sedimenten. Enke,
618 Stuttgart
619 Mehling. H., Hautzinger, G., Nilsson, O., Fricke, J., Hofmann, R., and Hahn, O. (1998) Thermal
620 diffusivity of semitransparent materials determined by the laser-flash method applying a new
621 mathematical model. International Journal of Thermophysics, 19, 941-949.
622 Mysen, B.O. and Richet, P. (2005) Silicate Glasses and Melts: Properties and Structure, 560 p.
623 Elsevier, Amsterdam.
624 Nabelek, P.I., Whittington, A.G., and Hofmeister, A.M. (2012) The influence of temperature-
625 dependent thermal diffusivity on the conductive cooling rates of plutons and temperature-
626 time paths in contact aureoles. Earth and Planetary Science Letters, 317-318, 157-164.
627 Neuville, D., Courtial, P., Dingwell, D., and Richet, P. (1993) Thermodynamic and rheological
628 properties of rhyolite and andesite melts. Contributions to Mineralogy and Petrology, 113, 572-
629 581.
630 Okamura, S., Nakamura, M., and Nakashima, S. (2003) Determination of molar absorptivity of IR
631 fundamental OH-stretching vibration in rhyolitic glasses. American Mineralogist, 88, 1657-1662.

632 Parker, J,W,, Jenkins, J.R., Butler, P.C., and Abbott G.I. (1961) Flash method of determining
633 thermal diffusivity, heat capacity, and thermal conductivity. Journal of Applied Physics. 32,
634 1679–1684.
635 Pertermann. M., Whittington, A.G., Hofmeister, A.M., Spera, F.J., and Zayak, J. (2008) Thermal
636 diffusivity of orthoclase glasses and single-crystals at high temperatures. Contributions to
637 Mineralogy and Petrology, 155, 689-702. doi, 10.1007/s00410-007-0265-x
638 Philpotts, J.A, and Pinson, W.H. (1966) New data on the chemical composition and origin of
639 moldavites. Geochimica Cosmochimica Acta 30, 253-266.
640 Pilkington, L.A.B. (1969) The float glass process. Proceedings of the Royal Society of London,
641 A314, 1-25.
642 Plazek. D.J. and Ngai, K.L. (1991) Correlation of polymer segmental chain dynamics with
643 temperature dependent time-scale shifts. Macromolecules, 24, 1222–1224.
644 Richet, P. (1984) Viscosity and configurational entropy of silicate melts. Geochimica Cosmochimica
645 Acta, 48, 471-483.
646 Richet, P. (1987) Heat capacity of silicate glasses. Chemical Geology, 62, 111-124.
647 Richet. P. and Bottinga, Y. (1995) Rheology and configurational entropy of silicate melts. Reviews
648 in Mineralogy, 32, 67-93.
649 Richet, P., Robie, R.A., and Hemingway, B.S. (1986) Low-temperature heat capacity of diopside
650 glass ($CaMgSi_2O_6$), a calorimateric test of the configurational entropy theory applied to the
651 viscosity of liquid silicates. Geochimica Cosmochimica Acta, 50, 1521-1533.
652 Romine. W,L., Whittington, A.G., Nabelek, P.I., and Hofmeister,.A.M. (2012) Thermal
653 diffusivity of rhyolitic glasses and melts, effects of temperature, crystals and dissolved water.
654 Bulletin of Volcanology, 74, 2273-2287.

655 Rossman, G.R. (1988a) Vibrational spectroscopy of hydrous components. Reviews in Mineralogy,
656 18, 191-206.
657 Rossman, G.R .(1988b) Optical Spectroscopy. Reviews of Mineralogy, 18, 207-254.
658 Russell, J.K., Giordano, D., and Dingwell, D.B. (2003) High-temperature limits on viscosity of non-
659 Arrhenian silicate melts. American Mineralogist, 88, 1390–1394.
660 Shelby, J.E. (2005) Introduction to Glass Science and Techology. Royal Society of Chemistry,
661 Cambridge.
662 Shibata, H., Suzuki, A., and Ohta, H. (2005) Measurement of thermal transport properties for
663 molten silicate glasses at high temperatures by means of a novel laser flash technique.
664 Materials Transactions, 46, 1877-1881.
665 Stebbins. J.F., Carmichael, I.S.E., and Moret, L.K. (1984) Heat capacities and entropies of
666 silicate liquids and glasses. Contributions to Mineralogy and Petrology, 86, 131-148.
667 Stebbins J.R., McMillan, P.F., and Dingwell, D.B. (1995) Structure, dynamics and properties of
668 silicate melts. In, Ribbe PH (ed) Reviews in Mineralogy, Vol. 32.
669 Stolper, E. (1982) Water in silicate glasses, an infrared spectroscopic study. Contributions to
670 Mineralogy and Petrology, 81, 1-17.
671 Tang, X. and Dong, J.J. (2010), Lattice thermal conductivity of MgO at conditions of Earth's
672 interior. Proceedings of the National Academy of Science, 107, 4539–4543.
673 Toplis, M.J. and Dingwell, D.B. (2004) Shear viscosities of CaO-Al_2O_3-SiO_2 and MgO-Al_2O_3-SiO_2
674 liquids, implications for the structural role of aluminium and the degree of polymerisation of
675 synthetic and natural aluminosilicate melts. Geochimica Cosmochimica Acta, 68, 5169-5188.
676 Toplis, M.J. and Richet, P. (2000) Equilbrium density and expansivity of silicate melts in the glass
677 transition range. Contributions to Mineralogy and Petrology, 139, 672-683.

678 Vo-Thanh, D., Polian, A., Richet, P. (1996) Elastic properties of silicate melts up to 2350 K from
679 Brillouin scattering. Geophysical Research Letters, 23, 423-426.
680 Whittington, A., Richet, P., Behrens, H., Holtz, F., and Scaillet, B. (2004) Experimental
681 temperature-X(H_2O)-viscosity relationship for leucogranites, and comparison with synthetic
682 silicic liquids. Trans Royal Soc Edinburough, Earth Science 95, 59-72.
683 Whittington, A.G., Bouhifd, M.A., and Richet, P. (2009a) The viscosity of hydrous $NaAlSi_3O_8$ and
684 granitic melts, configurational entropy models. American Mineralogist 94, 1-16.
685 Whittington, A.G., Hellwig, B.M., Behrens, H., Joachim, B., and Stechern, A. (2009b) The viscosity of
686 hydrous dacitic liquids, implications for the rheology of evolving silicic magmas. Bulletin of
687 Volcanology, 71, 185-199.
688 Whittington, A.G., Richet, P., and Polian, A. (2012) Water and the compressibility of silicate glasses: a
689 Brillouin spectroscopic study. American Mineralogist, 97, 455-467.
690 Yu, X. and Hofmeister, A.M. (2011) Thermal diffusivity of alkali and silver halides. Journal of
691 Applied Physics, 109, locator number 033516
692

693 FIGURE CAPTIONS

694 **Fig. 1.** Unpolarized absorption spectra of the O-H fundamental region for selected samples.
695 Thicknesses of the samples (*L*) are labeled but spectra as shown are scaled to represent 1 mm
696 thickness. Baseline corrections are not shown. Due to imperfect surface polish, true absorbance
697 near 4000 cm^{-1} is zero. Grey = natural samples with similar patterns (dashed = indochinite; solid
698 = moldavite; dots = spectra from a 4.4 mm Al-rich rhyolite). The rise to high frequency is due to
699 Fe^{2+} transitions. Black = effect of heating on 1926 window glass, which has the same profile as
700 the other Na-Ca commercial glasses. The rise to high ν for heated samples (from L = 0.9 mm) is

due to imperfect surface polish. Thickness was 2.4 mm for the fresh sample. Overtones of Si-O lattice modes are near 2400 cm^{-1}.

Fig. 2 Unpolarized absorption spectra of d-d electronic transitions of Fe ions. Thicknesses of the samples (*L*) are labeled but spectra as shown are scaled to represent 1 mm thickness. **(a)** Near-IR data, as labeled, on ferrous iron in octahedral coordination. Light vertical lines show that the same positions exist for the high Al glasses, but that the Ca-rich glasses have broader bands. Thickness was 2.7 and 3.5 mm for the high and low frequency spectral segments of 1895. **(b)** Visible-UV region showing ferric iron, if present. For the thin curves, solid line = 1895 from thickness of 0.10 mm for the UV and 2.705 mm for the visible; dotted line = 1960 with L= 0.787 to 0.917 mm; dashed line = "modern" with L = 1.124 mm; dot-dashed line =1926 from L = 0.608 to 0.848 mm. * = Fe^{3+} transitions in a tetrahedral site. Vertical line = Fe^{2+} transitions in a tetrahedral site or intervalence charge transfer (IVCT). Double vertical line indicates Fe^{2+} in an octahedral site.

Fig. 3. Viscosity data for supercooled liquids near the glass transition. Lines are TVF curves. Filled symbols listed on left = Al-rich samples. Open symbols listed on right = Na-Ca samples. Leucogranite data from Whittington et al. (2009a).

Fig. 4. Thermal diffusivity, comparison of high-Al rhyolite to Na-Ca glasses and liquids. Symbols are the average of 3 datapoints (>6 at room temperature). Double arrow = transition interval. Curves are fits in Table 5 and 6, unless stated otherwise. Dots = remelted rhyolite as quenched for two different discs. The three different pieces represent varying amounts of residual strain. The fit is to all data. Squares = modern Na-Ca glass, fit by $D = 1.00T^{-0.124}$, Open squares = modern liquid. Diamonds = vase, was fit by $D = 1.18T^{-0.155}$. Open diamonds = vase liquid. + = 1890. X = 1884. Flow (sagging) onsets above 1200 K.

724 **Fig. 5.** Thermal diffusivity vs. temperature. **(a)** Antique and modern commercial samples with
725 high Na contents, showing power law fits. Triangles = 1895 which melted gradually, then
726 flowed at the highest temperature accessed. Two sequential runs are shown for disc #1 of 1960
727 (filled squares, crossed squares). A fit was not made to data for the dry sample because data
728 points were widely spaced. Filled diamonds = a second disc from 1960. **(b)** 1926 with power
729 law fits as labeled. The wide variation in *D* is attributed to strain in this rolled glass. **(c)** Granitic
730 glasses and liquids. Filled and open square = 1st sample of haplogranite. Square with plus = 2nd
731 sample of haplogranite. Leucogranite (diamonds) has much higher Fe content. Just above
732 melting, leucogranite *D* increased slightly, connected with degassing. **(d)** Tektites and Al-
733 rhyolite with K>Na. Above T_g moldavite back transformed to glass, attributed to loss of water.
734 **Fig. 6.** Dependence of thermal diffusivity on chemical composition. Circles = *D* at 298 K.
735 Squares = *D* upon melting. Also included are data from Hofmeister et al. (2009). Dotted and
736 dashed lines are linear fits. Solid lines are trends within the Al-rich glasses and liquids. **(a)** *D* vs
737 Al content per 8 O atoms **(b)** *D* vs. Ca content per 8 atoms. Alkali feldspar melts (square with
738 plus) are not included in the fit.
739 **Fig. 7.** Dependence of thermal diffusivity of glasses and liquids on physical properties.
740 Additional data from Pertermann et al. (2008); Hofmeister et al. (2009); Whittington and
741 Hofmeister (2012). **(a)** *D* of glass and melt vs. fragility. Symbols for liquid are as labeled,
742 except unlabeled crossed squares are alkali feldspar melts. For glass, the same symbols are used,
743 but are grey. Lines are not fits, but indicate ranges of values. **(b)** *D* upon melting vs. density.
744 **Fig. 8.** Thermal conductivity. Lines are labeled, such that heavier weight lines represent liquid.
745 (**a**) Soda-lime compositions, for which melt density is well-known. (**b**) Al-rich samples, for
746 which we assumed $\alpha_{glass} = 20\times10^{-6}$ K^{-1}, as measured for phonolitic glass (Bouhifd et al. 2001).

747 **Fig. 9.** Ternary diagrams of thermal diffusivity for common igneous melts. Left = felsic rocks.
748 Right = mafic rocks. Letters indicate samples of (I) indochinite, (M) moldavite, (R) rhyolite, (L)
749 leucogranite and (H) haplogranite. Other labels indicate melts of mineral stoichiometry. Olivine
750 melt was projected using Fig. 7.
751

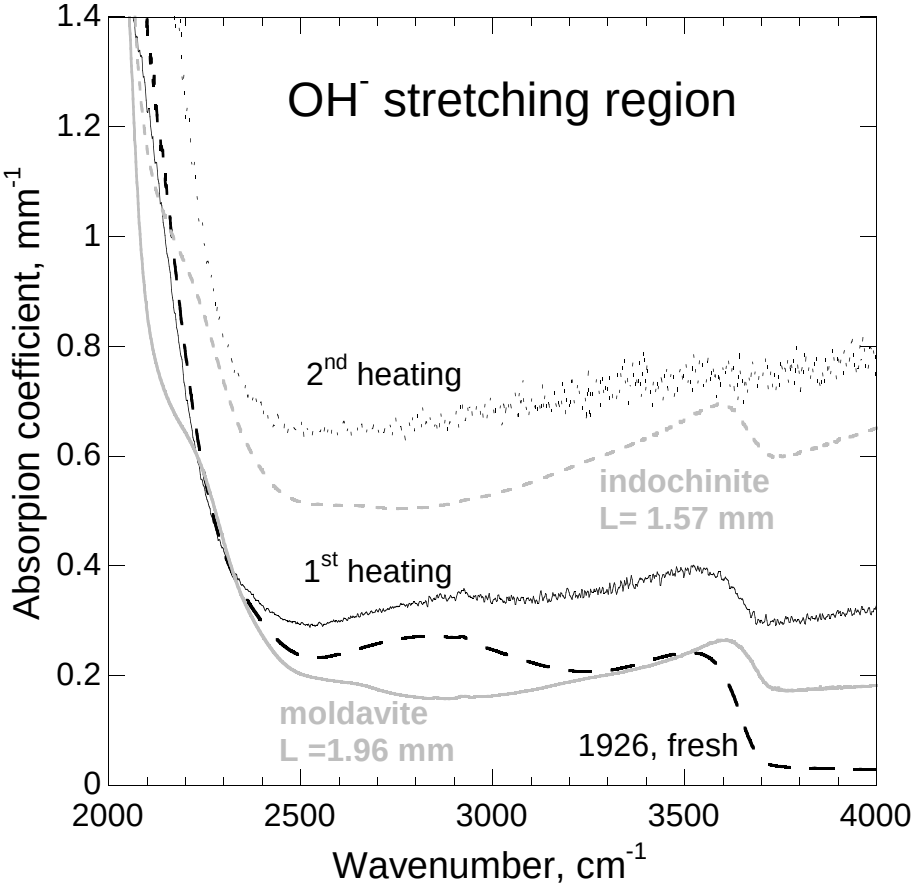
OH- stretching region
2nd heating
indochinite
L= 1.57 mm
1st heating
moldavite
L =1.96 mm
1926, fresh
Absorpion coefficient, mm-1
Wavenumber, cm-1
0
0.2
0.4
0.6
0.8
1
1.2
1.4
2000
2500
3000
3500
4000

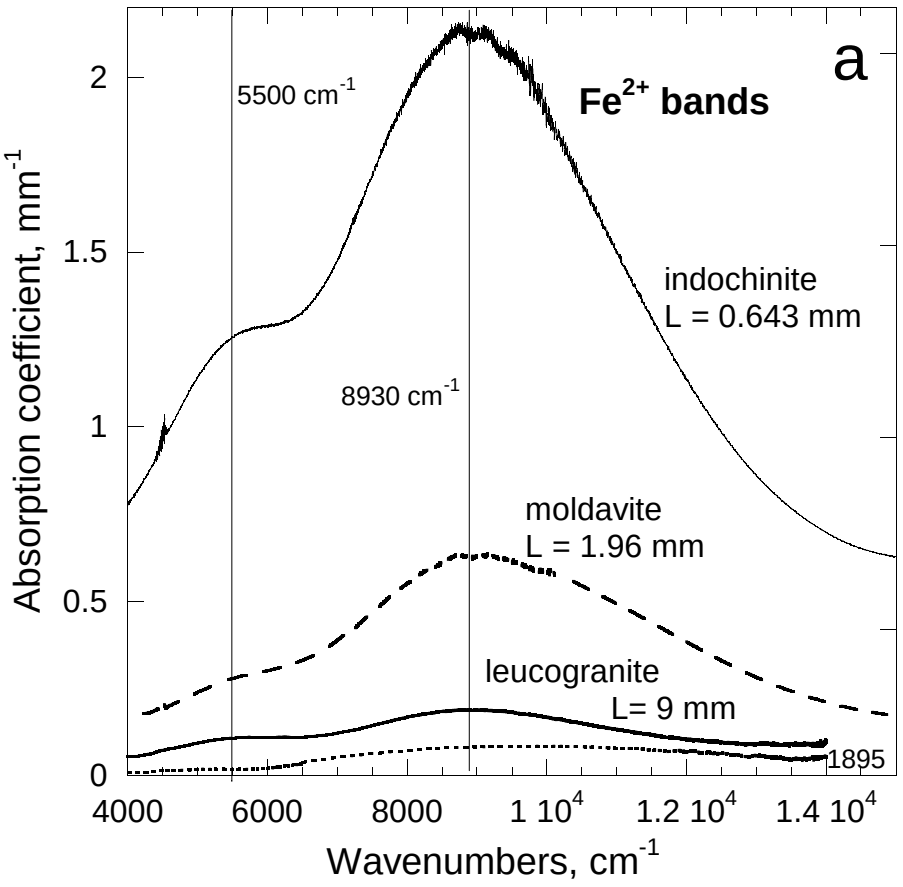
a
Fe2+ bands
5500 cm-1
8930 cm-1
indochinite
L = 0.643 mm
moldavite
L = 1.96 mm
leucogranite
L= 9 mm
1895
Absorption coefficient, mm-1
Wavenumbers, cm-1
0
0.5
1
1.5
2
4000
6000
8000
1 10^4
1.2 10^4
1.4 10^4

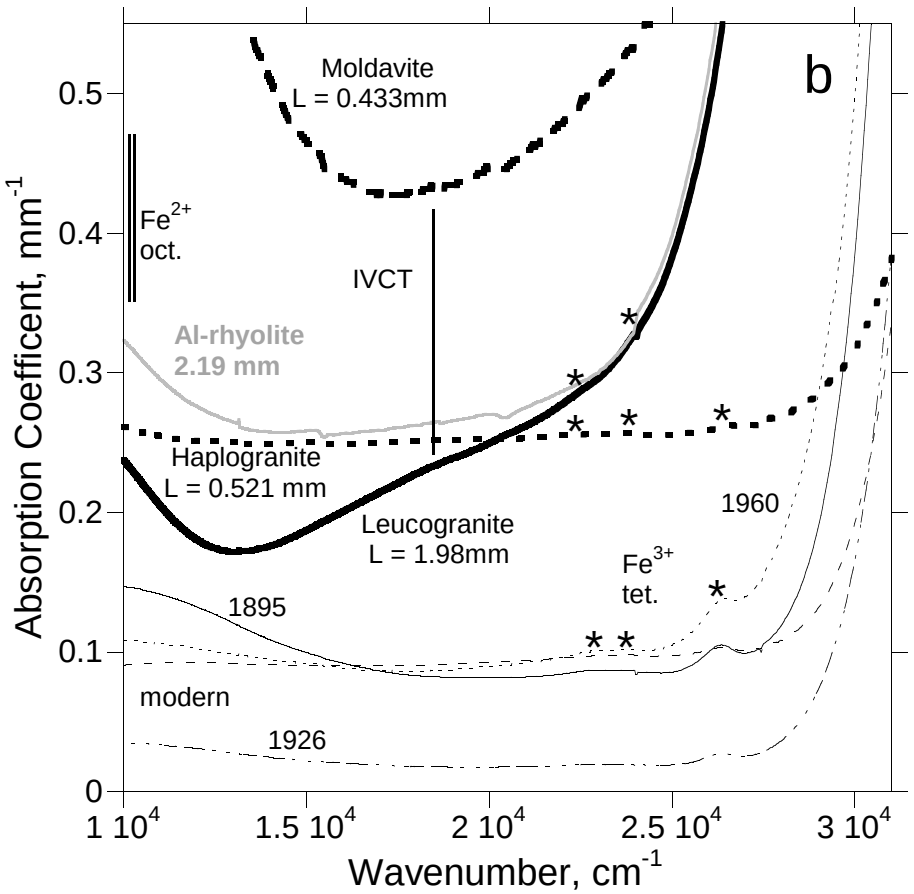
b
Moldavite
L = 0.433mm
Fe2+
oct.
IVCT
Al-rhyolite
2.19 mm
Haplogranite
L = 0.521 mm
Leucogranite
L = 1.98mm
1960
Fe3+
tet.
1895
modern
1926
Absorption Coefficent, mm-1
Wavenumber, cm-1
0
0.1
0.2
0.3
0.4
0.5
1 10^4
1.5 10^4
2 10^4
2.5 10^4
3 10^4

1000 900 800 700 600 500˚C

haplogranite
leucogranite
moldavite
indochinite
1926
vase
1960
1895

log viscosity (Pa s)

14.5 14.0 13.5 13.0 12.5 12.0 11.5 11.0 10.5 10.0 9.5 9.0 8.5 8.0

7.0 7.5 8.0 8.5 9.0 9.5 10.0 10.5 11.0 11.5 12.0 12.5 13.0

10000/T

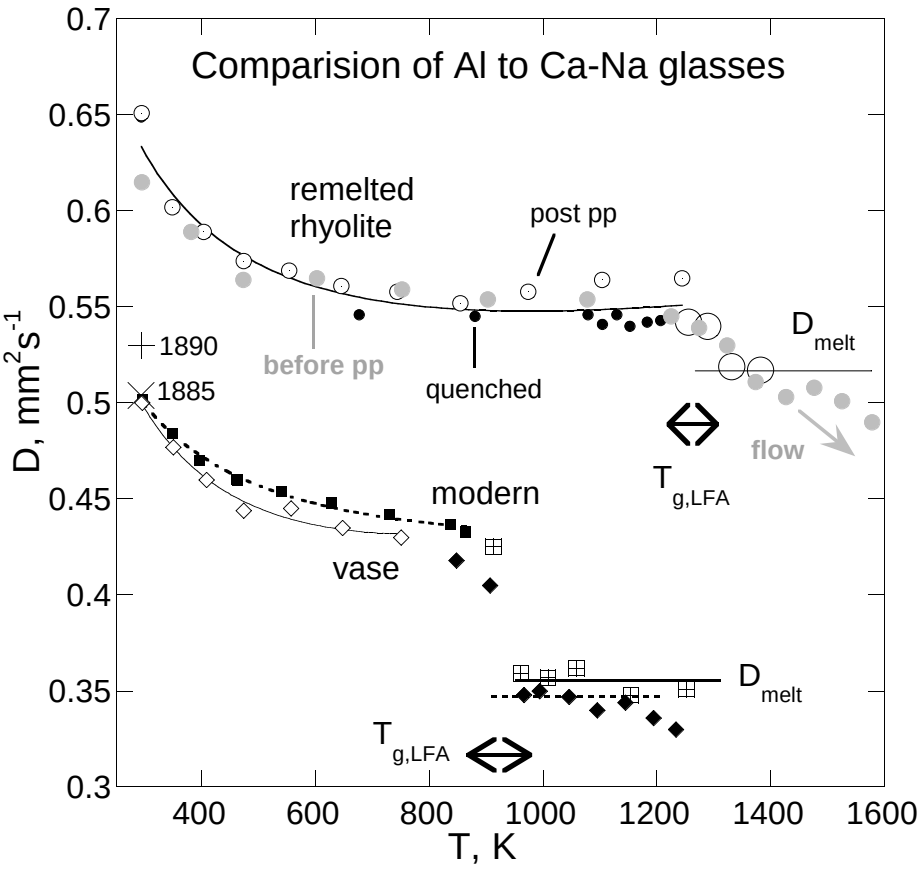
Comparision of Al to Ca-Na glasses
remelted
rhyolite
post pp
before pp
quenched
D melt
flow
T g,LFA
1890
1885
modern
vase
D melt
T g,LFA
D, mm2s-1
T, K
0.7
0.65
0.6
0.55
0.5
0.45
0.4
0.35
0.3
400
600
800
1000
1200
1400
1600

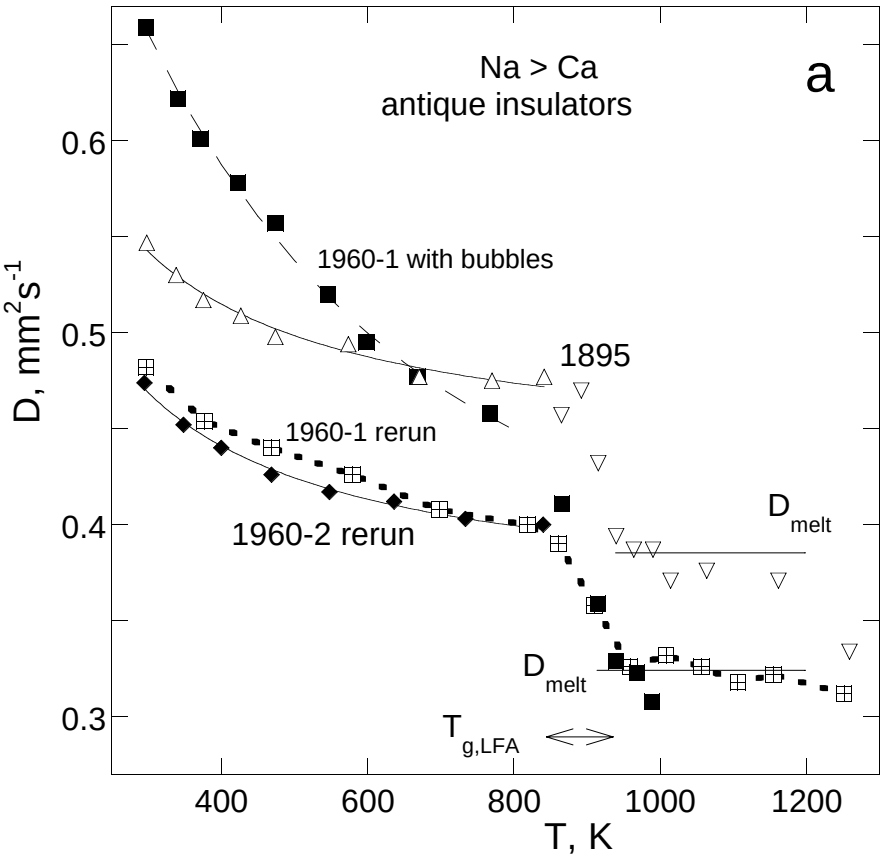
Na > Ca
antique insulators
a
1960-1 with bubbles
1895
1960-1 rerun
1960-2 rerun
D melt
D melt
T g,LFA
D, mm2s-1
T, K
0.3
0.4
0.5
0.6
400
600
800
1000
1200

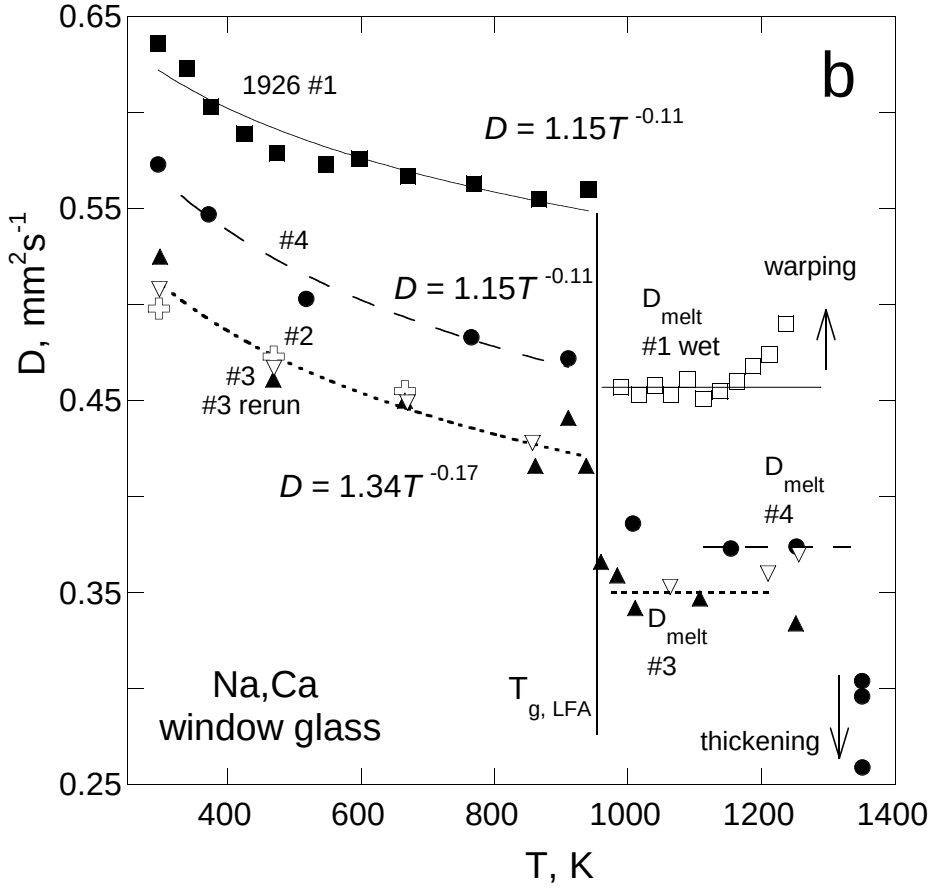
b
1926 #1
D = 1.15T -0.11
#4
D = 1.15T -0.11
#2
#3
#3 rerun
D = 1.34T -0.17
warping
D melt
#1 wet
D melt
#4
D melt
#3
Na,Ca
window glass
T g, LFA
thickening
D, mm2s-1
T, K
0.65
0.55
0.45
0.35
0.25
400
600
800
1000
1200
1400

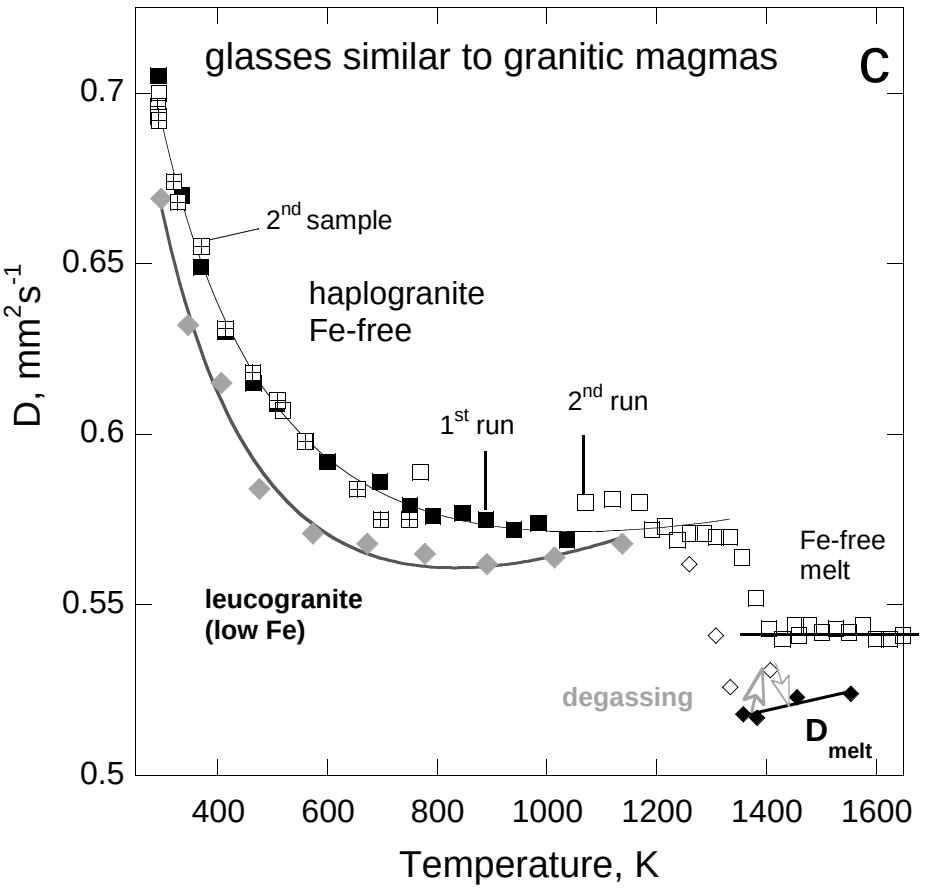
glasses similar to granitic magmas
C
0.7
0.65
0.6
0.55
0.5
D, mm2s-1
2nd sample
haplogranite
Fe-free
1st run
2nd run
Fe-free
melt
leucogranite
(low Fe)
degassing
Dmelt
400
600
800
1000
1200
1400
1600
Temperature, K

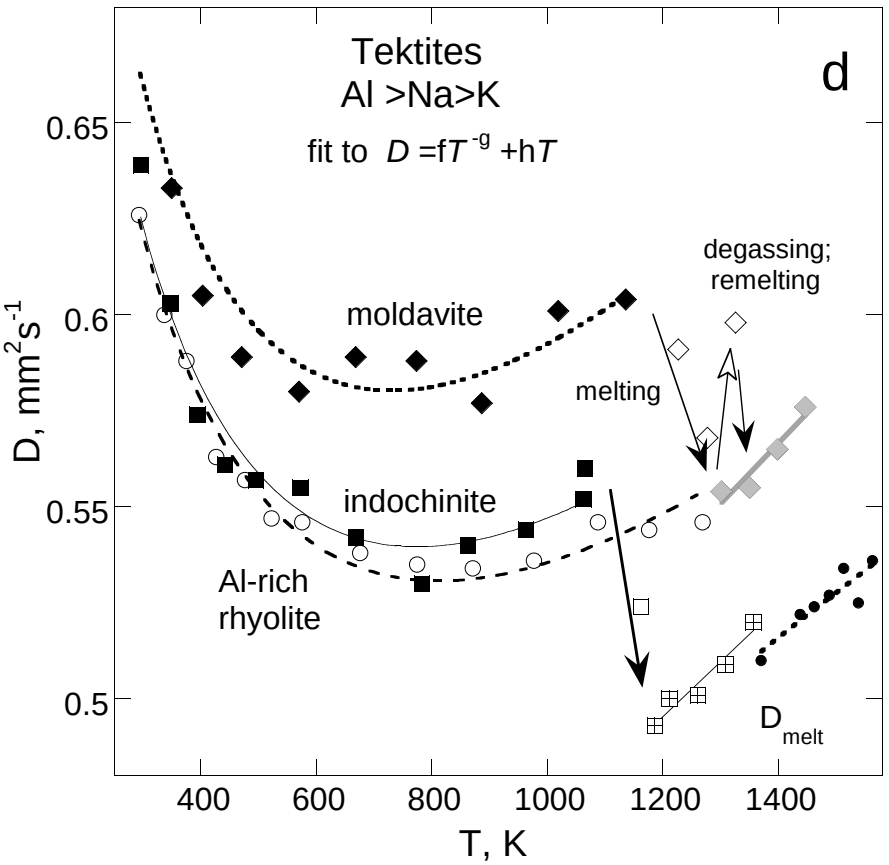
Tektites
Al >Na>K
fit to D =fT -g +hT
d
0.65
0.6
0.55
0.5
D, mm2s-1
moldavite
degassing;
remelting
melting
indochinite
Al-rich
rhyolite
D melt
400
600
800
1000
1200
1400
T, K

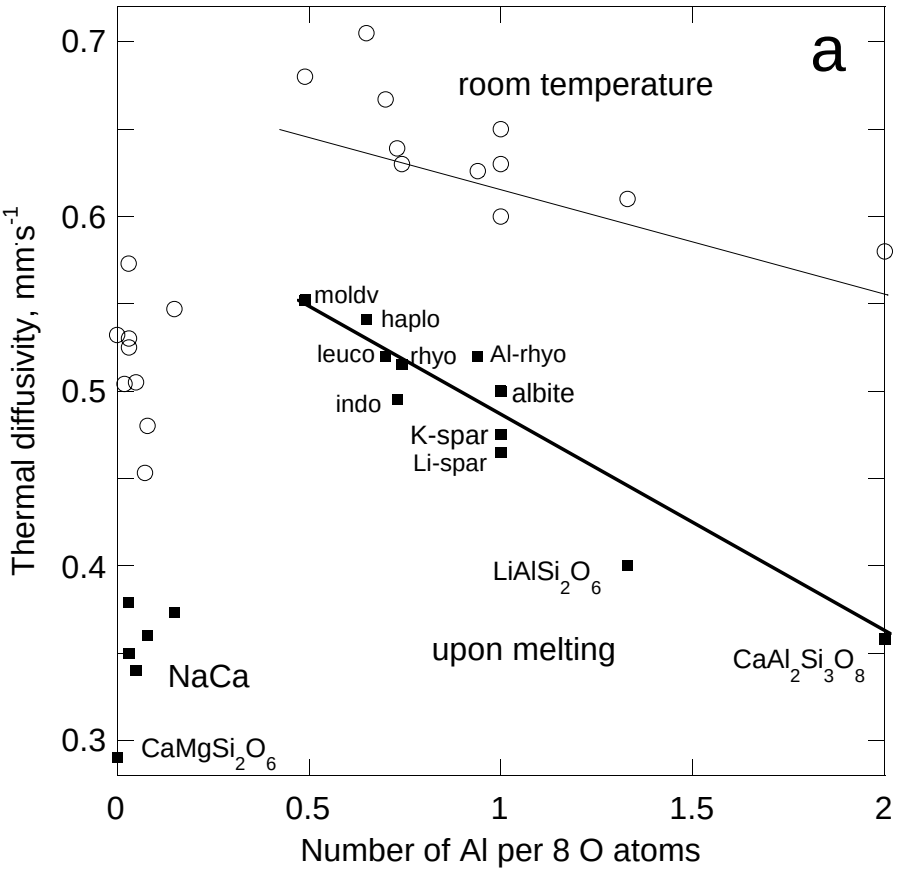
a
room temperature
upon melting
moldv
haplo
leuco
rhyo
Al-rhyo
albite
indo
K-spar
Li-spar
LiAlSi2O6
CaAl2Si3O8
NaCa
CaMgSi2O6
Thermal diffusivity, mm²s⁻¹
Number of Al per 8 O atoms
0.7
0.6
0.5
0.4
0.3
0
0.5
1
1.5
2

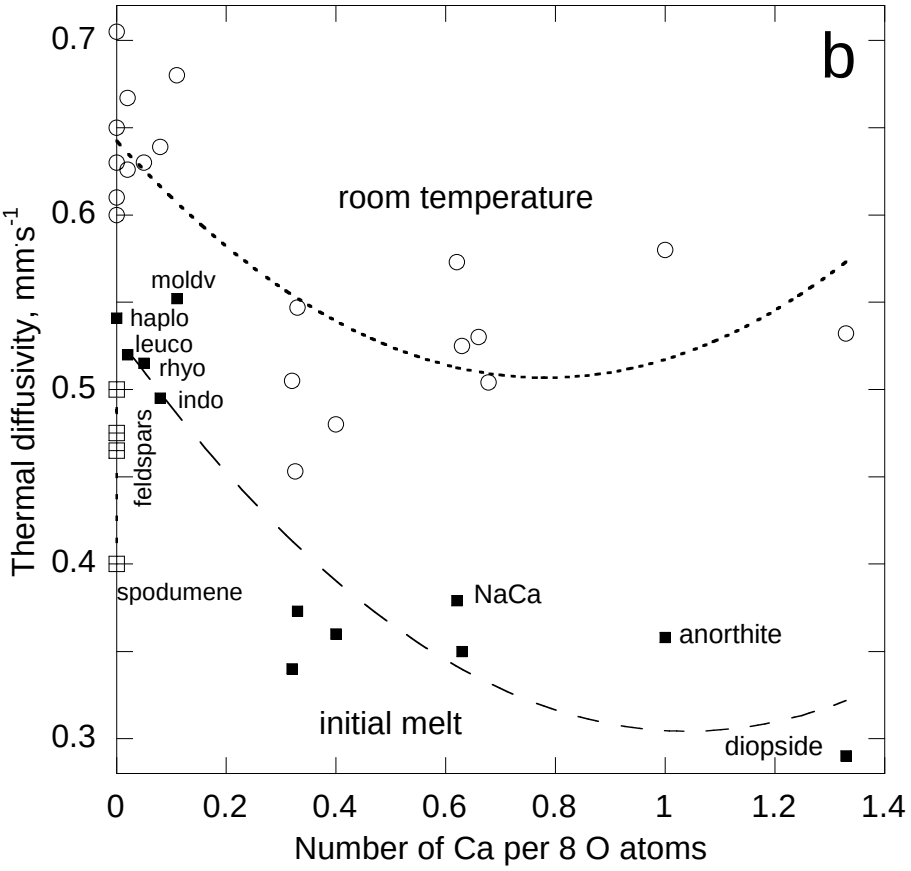
b
room temperature
initial melt
moldv
haplo
leuco
rhyo
indo
feldspars
spodumene
NaCa
anorthite
diopside
Thermal diffusivity, mm·s-1
Number of Ca per 8 O atoms
0.7
0.6
0.5
0.4
0.3
0
0.2
0.4
0.6
0.8
1
1.2
1.4

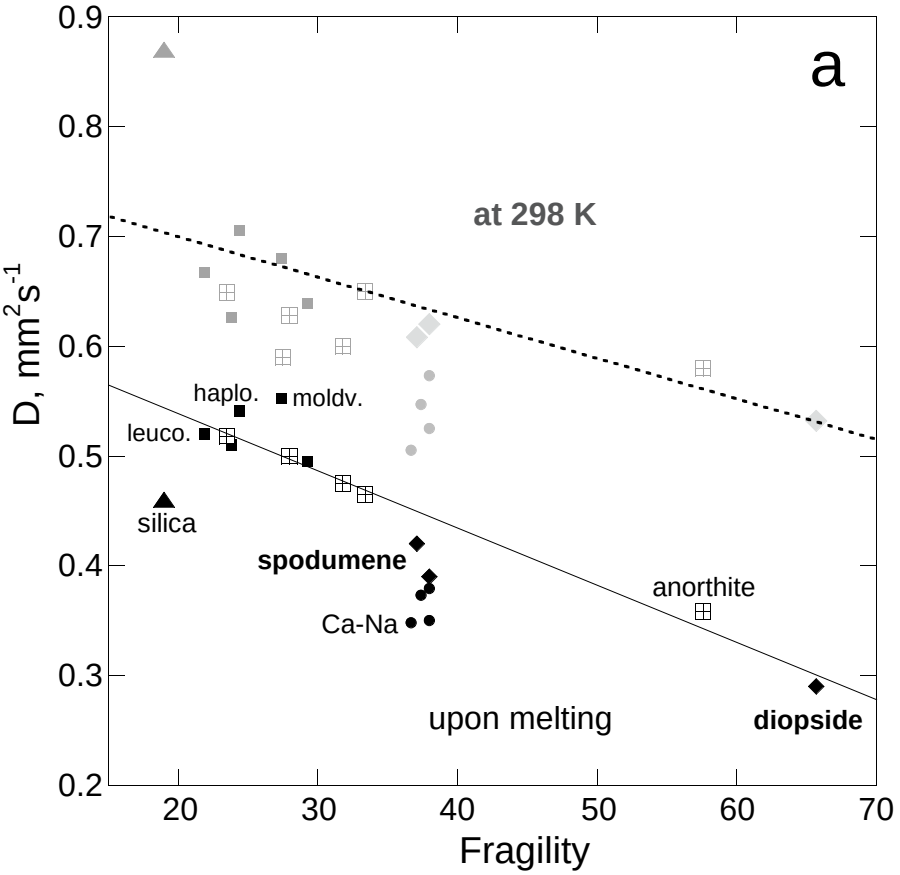
a
at 298 K
upon melting
haplo.
moldv.
leuco.
silica
spodumene
Ca-Na
anorthite
diopside
D, mm^{2}s^{-1}
Fragility
0.9
0.8
0.7
0.6
0.5
0.4
0.3
0.2
20
30
40
50
60
70

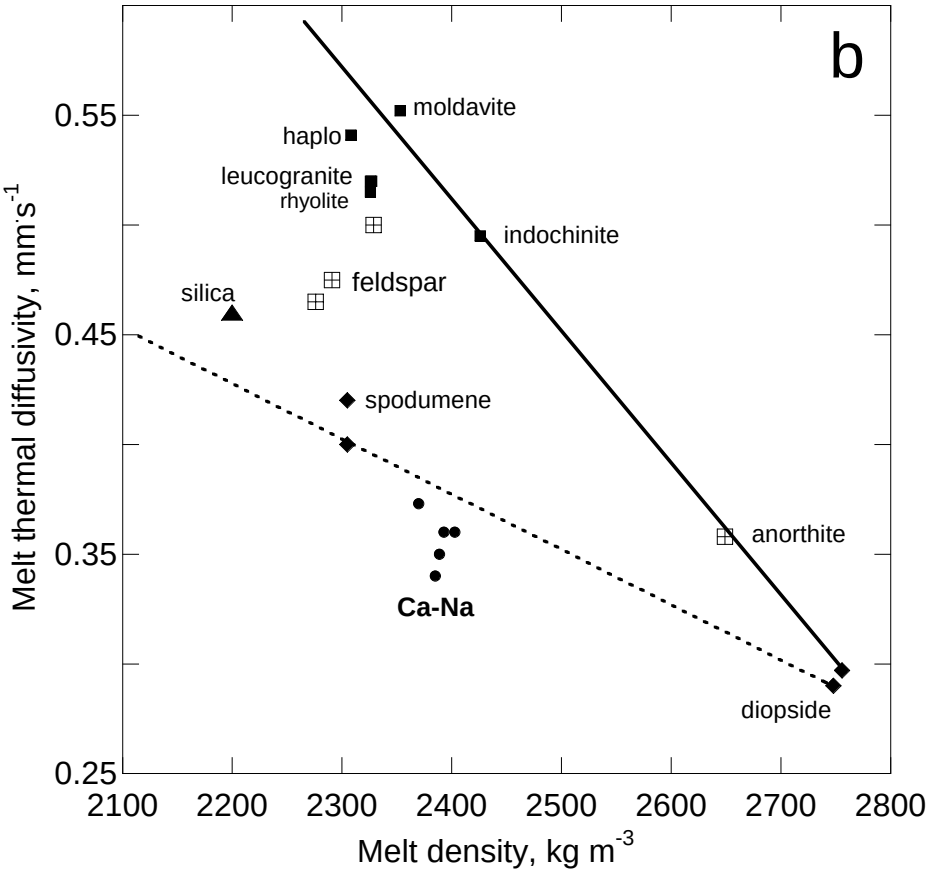
b
moldavite
haplo
leucogranite
rhyolite
indochinite
feldspar
silica
spodumene
anorthite
Ca-Na
diopside
0.55
0.45
0.35
0.25
2100
2200
2300
2400
2500
2600
2700
2800
Melt thermal diffusivity, mm˙s-1
Melt density, kg m-3

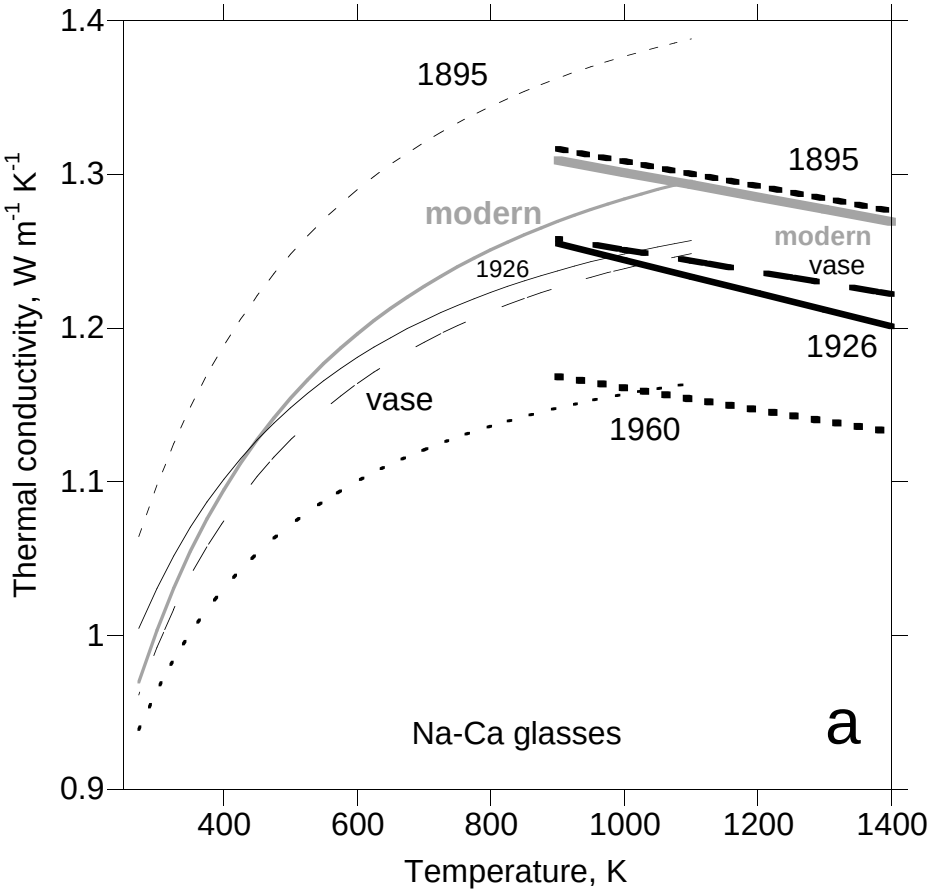
1.4
1.3
1.2
1.1
1
0.9
Thermal conductivity, W m-1 K-1
400
600
800
1000
1200
1400
Temperature, K
1895
1895
modern
modern
vase
1926
1926
vase
1960
Na-Ca glasses
a

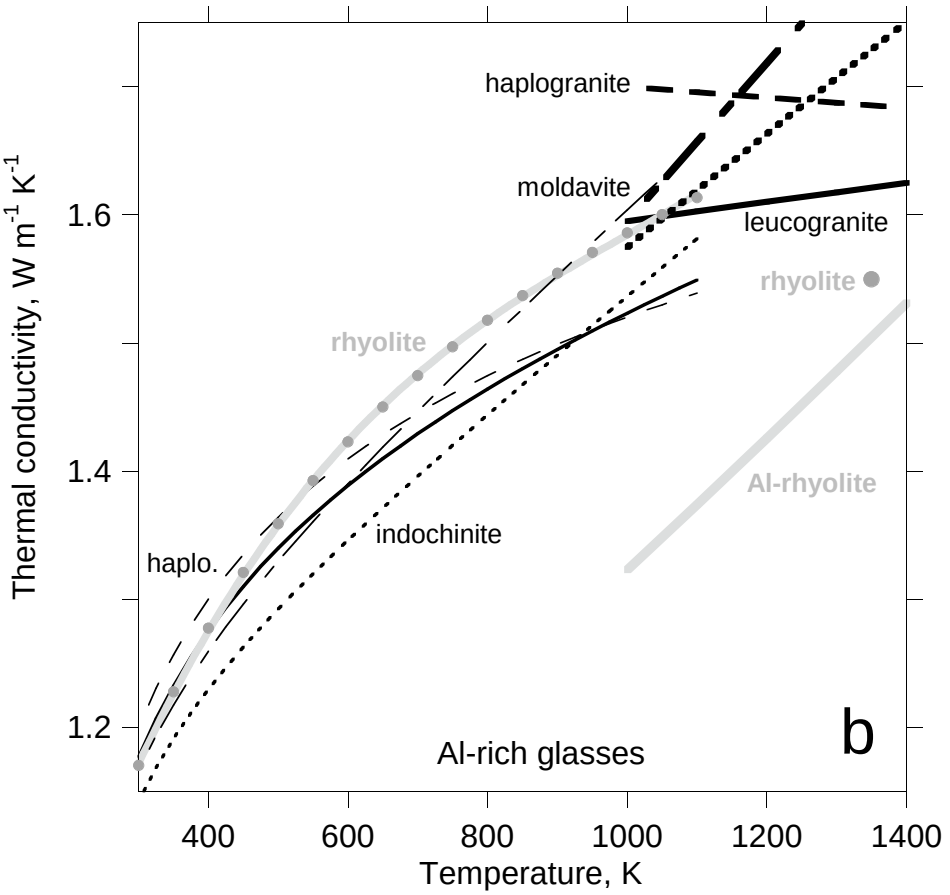
haplogranite
moldavite
leucogranite
rhyolite
rhyolite
Al-rhyolite
indochinite
haplo.
Al-rich glasses
b
Thermal conductivity, W m-1 K-1
1.2
1.4
1.6
400
600
800
1000
1200
1400
Temperature, K

FIGURE 9

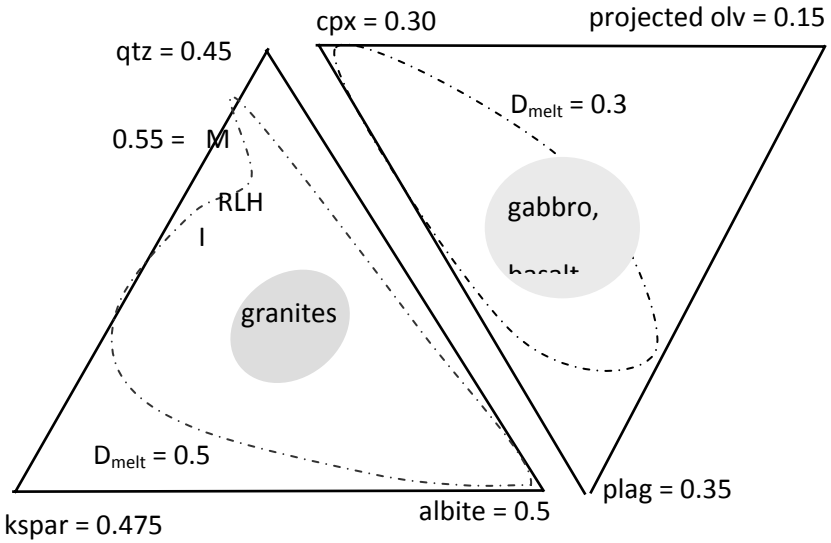
cpx = 0.30
projected olv = 0.15
qtz = 0.45
D_{melt} = 0.3
0.55 = M
RLH
I
gabbro,
granites
D_{melt} = 0.5
plag = 0.35
albite = 0.5
kspar = 0.475

Table 1. Sample descriptions

Sample	Key elements*	Density kg m^{-3}	Origin and/or Source	Color†	"Formula"*
1895	high Na>Ca	2480	antique insulator from telephone line‡	aqua blue	$Na_{1.40}K_{0.05}Ca_{0.33}Mg_{0.10}Fe_{0.02}Al_{0.15}Si_{3.30}O_8$
1960	high Na>Ca	2476	antique insulator from telephone line§	colorless	$Na_{1.37}Ca_{0.306}Mg_{0.289}Al_{0.053}Si_{3.32}O_8$
Vase	Na>Ca	2475	vase from an antique store‖	colorless	$Na_{1.25}K_{0.018}Ca_{0.326}Mg_{0.313}Al_{0.073}Si_{3.305}O_8$
Modern	Na>Ca	2491	ground glass from Edmund Scientific	colorless	$Na_{1.21}Ca_{0.40}Mg_{0.31}Al_{0.08}Si_{3.28}O_8$
1884	Na>~Ca	2533	antique window pane@	colorless	$Na_{1.22}K_{0.005}Ca_{0.678}Mg_{0.025}Fe_{0.005}Al_{0.028}Si_{3.315}O_8$
1890	Na>~Ca	n.d.	antique window pane#	colorless	$Na_{1.12}K_{0.007}Ca_{0.660}Mg_{0.025}Fe_{0.007}Al_{0.031}Si_{3.327}O_8$
1926	Na>~Ca	2498	antique window pane¶	colorless	$Na_{1.08}Ca_{0.61}Al_{0.03}Si_{3.39}O_8$
Haplogranite	Al>Na>K	2276	laboratory synthetic	colorless	$Na_{0.34}K_{0.24}Al_{0.65}Si_{3.35}O_8$
Leucogranite	Al>Na~K	2338	remelt	pale brown	$Na_{0.27}K_{0.25}Ca_{0.02}Fe_{0.04}Al_{0.70}Si_{3.31}O_8$
Rhyolite	Al>Na>K	2350	remelt	light brown	$Na_{0.36}K_{0.29}Ca_{0.05}Fe_{0.04}Al_{0.74}Si_{3.73}O_8$
Al-rhyolite	Al>K>Na	2350	remelt, Al contaminated	light brown	$Na_{0.23}K_{0.41}Ca_{0.02}Fe_{0.03}Al_{0.94}Si_{3.60}O_8$
Moldavite	Al>K~Mg	2343	Habri, Czech Republic, from Excaliber	green	$Na_{0.09}K_{0.19}Ca_{0.11}Mg_{0.12}Fe_{0.05}Al_{0.49}Si_{3.44}O_8$
Indochinite	Al>Fe~K~Mg	2425	Kohn Khaen, Thailand, Ebay purchase	dark brown	$Na_{0.03}K_{0.14}Ca_{0.08}Mg_{0.13}Fe_{0.18}Al_{0.73}Si_{3.20}O_8$

Notes: For the antiques, the sample number is the year of manufacture, if known. The remelted rhyolites are samples NCAR (rhyolite) and NCr (Al-rhyolite) described by Romine et al. (2012). The last digits are uncertain.

*Detailed in text and tables. Cations most abundant after Si are listed. The commercial glasses with significant Ca have two sites for OH^-. "Formula" are given for comparison with glasses previously studied. Trace Ti is grouped with Si.

†Color is related to presence of Fe^{3+}

‡Manufactured at the Hemingray factory in Covington, KY between 1894 and 1895. Commonly produced in blue to green hues, due to use of sand from dunes at Michigan Beach, Michigan which are impure. At this time, recycled glass was often added to the vats to reduce cost. Many bubbles are present due to crude molding techniques and furnace temperatures being close to glass melting temperature. Found in Missouri.

§Among the last glass made at the Hemingray factory located in Muncie, IN. Embossed with year of manufacture. At this time Hemingray Co. primarily produced glass windows and blocks for residential use, using pure quartz sandstone. Few bubbles are present due to mechanized molding techniques and furnace temperatures well exceeding glass melting temperature. Found at a farm in south central Ohio.

||This vase was purchased at Treasure Isles Antique Mall, 2317 South Big Bend Blvd. St. Louis MO 63143 USA. Its probable date of manufacture lies between the 1930's thru 1960's.

@ From the ruins of the National Memorial Church of God in Christ, located at 460 North Spring Avenue, St. Louis MO USA. Completed in 1884, the church burned down in 2001, only the exterior remains are still standing. The glass sample was in hte soil beneath one of the windows.

#From the ruins of the Sheahan Quarries private railroad engine house located in Elephant Rocks State Park, MO USA. Constructed during the 1890's this structure was created out of the same granite which was being quarried at the site. The glass sample was dug out of the soil directly beneath an opening in the side wall where the window and floor used to exist.

¶ Date reflects construction of the depression era house at 2561 Circle Dr., Maplewood MO. Manufactured using a plate glass process, because the float glass technique originated subsequently (Pilkington, 1969) and the appearance is slightly wavy, like that of rolled glass. Few impurities exist due to use of mined quartz sandstones.

Table 2. Chemical compositions (in wt %) and hydroxyl contents (in ppm by wt)

	1895	1960	Vase	Modern	1884	1890	1926-1[f]	1926-3	1926-4	Haplo.	Leuco.	Moldv.	Indoc.
SiO_2	72.59	72.91	72.99	71.73	71.39	72.2-72.5	74.34	74.70	75.50	79.63	77.72	80.25	72.19
TiO_2	0.10	0.01	0.01	0.05	0.06	0.01-0.03	0.054	0.03	0.05	0.018	0.073	0.30	0.81
Al_2O_3	2.85	0.98	1.38	1.45	0.05	0.73-0.41	0.43	0.44	0.44	13.35	13.80	9.86	14.16
Cr_2O_3	n.d.	0.003	0.010	b.l.d	0.003	b.l.d.	0.004	0.006	b.l.d	0.007	b.l.d	0.005	0.016
FeO	0.36	0.02	0.03	0.075[d]	0.13	0.25-0.08	0.18	0.11	0.13	0.05[d]	1.00	1.53	4.84
MnO	0.01	0.01	0.005	0.04	0.004	~0.01	0.01	0.01	0.002	0.007	0.058	0.06	0.11
MgO	1.50	4.12	4.64	4.49	0.37	0.26-0.45	0.45	0.45	0.50	0.064	0.039	1.87	2.01
CaO	6.69	6.28	6.72	8.22	13.62	13.2-13.6	12.20	12.60	12.60	0.038	0.46	2.46	1.80
Na_2O	15.95	15.49	14.33	13.66	13.56	13.2-12.0	12.77	12.03	12.00	4.23	3.26	0.37	1.07
K_2O	0.90	0.22	0.31	0.29	0.08	0.14-0.06	0.14	0.12	0.12	4.36	4.59	3.45	2.55
Sum	100.96	100.08[c]	100.41	100.00	99.27	99.7-100.5[e]	100.80	100.84	101.83	101.75	101.09	99.56	99.97
OH^-, ppm[a]	110	160	90	160	210	240	220	200	-	170	200	150	100
T~ 973 K	-	150	-	-	-	-	-	-	-	-	-	-	-
T>1273 K	-	-	-	-	-	22	120	~10	60	-	130	-	-
NBO/T[b]	0.63	0.75	0.73	0.77	0.79	0.74	0.70	0.68	0.68	0.00	0.00	0.07	0.07

Notes: Chemical analyses of the remelted rhyolites are provided by Romine et al. (2012). The last digit is uncertain, unless noted.

[a] OH^- contents determined initially and after LFA runs to the temperatures indicated. Initially, Al-rhyolite has 130 ppm OH, whereas rhyolite had 230 ppm (Romine et al. 2012).

[b]NBO/T is the nominal ratio of non-bridging oxygens to tetrahedral cations, calculated according to NBO/T = $(FeO+MnO+MgO+CaO+Na_2O+K_2O - 2Al_2O_3 - 2Cr_2O_3)/(SiO_2 + TiO_2 + 2Al_2O_3 + 2Cr_2O_3)$ on a molar basis, and using average compositions for the 1890 glass. For rhyolite and Al-rhyolite, NBO/T = 0.02 and 0, respectively.

[c] Includes 0.263 wt% SO_2 and 0.003 wt % V_2O_3.

[d] Contains only Fe^{3+}, whereas the remaining samples contain both Fe^{3+} and Fe^{2+}.

[e]Includes 0.05 wt% SO_2.

[f] Microprobe analysis after heating

Table 3a. Viscosity measurements: Ca-Na rich melts

1895		1926		1960		vase	
T	log η	T	log η	T	log η	T	log η
K	log Pa s	K	log Pa s	K	log Pa s	K	log Pa s
792.7	12.68	803.8	13.90	805.0	12.22	808.1	12.34
811.2	11.76	828.7	12.65	828.4	11.12	827.3	11.46
830.7	10.90	837.9	12.29	838.9	10.69	838.9	11.12
850.1	10.16	848.3	11.73	850.0	10.31	842.7	10.83
855.1	10.00	857.4	11.39	858.6	9.97	858.0	10.28
864.8	9.68	867.6	10.92	869.6	9.64	867.8	10.01
869.0	9.52	867.9	10.90	873.2	9.47	877.0	9.61
869.4	9.49	878.6	10.54	878.4	9.40	885.3	9.35
888.6	8.91	887.4	10.17	888.9	9.05	895.8	9.10
		906.8	9.52	892.6	8.89	914.1	8.57
				906.9	8.49	917.4	8.41

Notes: The last digit is uncertain.

Table 3b. Viscosity measurements: Al-rich melts

moldavite		indochinite		haplogranite		rhyolite		Al-rhyolite	
T	log η	T	log η	T	log η	T	log η	T	log η
K	log Pa s	K	log Pa s	K	log Pa s	K	log Pa s	K	log Pa s
1048.0	12.99	992.8	12.94	1160.9	11.61	1039.8	12.74	1130.3	11.59
1063.1	12.56	998.0	12.83	1170.7	11.43	1050.3	12.54	1130.6	11.69
1083.6	12.04	1006.8	12.46	1180.8	11.23	1069.7	12.07	1150.5	11.18
1098.6	11.68	1010.1	12.40	1181.5	11.23	1090.6	11.41	1150.8	11.28
1104.7	11.56	1019.4	12.11	1190.6	11.07	1110.6	11.02	1170.4	10.81
1113.3	11.30	1023.3	12.02	1190.8	11.06	1130.6	10.66	1170.8	10.89
1128.1	10.97	1027.0	11.93	1190.9	11.07	1130.7	10.90	1190.7	10.42
1144.1	10.71	1029.1	11.84	1198.5	10.93	1150.8	10.31	1190.9	10.53
1148.5	10.54	1038.1	11.61	1200.7	10.88	1170.7	9.99	1210.8	10.07
1168.6	10.15	1047.9	11.30	1201.5	10.91	1170.9	10.21	1211.0	10.18
1188.7	9.77	1048.9	11.35	1210.9	10.69	1190.8	9.68	1219.3	9.90
		1053.3	11.18	1218.2	10.59	1204.5	9.58	1231.0	9.73
		1057.7	11.11	1220.9	10.51	1205.6	9.46	1231.1	9.84
		1062.8	10.93	1221.0	10.56	1208.5	9.42	1239.0	9.58
		1067.7	10.82	1231.4	10.33	1226.0	9.19	1258.8	9.27
		1068.6	10.83	1234.8	10.30	1236.2	9.04	1261.0	9.34
		1070.0	10.80	1236.3	10.25	1694.5	4.50	1278.6	8.98
		1071.0	10.80	1239.4	10.18	1714.6	4.35	1280.8	9.05
		1078.2	10.61	1241.0	10.17	1723.9	4.30	1666.6	4.65
		1078.9	10.62	1241.6	10.22	1746.9	4.13	1674.9	4.59
		1083.2	10.45	1242.4	10.16	1753.2	4.09	1681.5	4.54
		1088.1	10.36	1242.8	10.18	1774.4	3.96	1696.1	4.42
		1088.5	10.39	1248.1	10.07			1710.8	4.31
		1098.4	10.11	1258.4	9.89			1725.5	4.19
		1108.4	9.94	1258.7	9.88			1735.3	4.13
		1108.6	9.91	1261.4	9.89			1740.5	4.09
		1113.4	9.79					1774.5	3.82
		1121.0	9.67						
		1123.0	9.55						
		1128.8	9.47						
		1130.1	9.50						
		1133.2	9.44						
		1143.2	9.25						
		1143.7	9.19						
		1159.4	8.90						
		1167.0	8.77						

Notes: Viscosity data for leucogranite are given by Whittington et al. (2009b). The last digit is uncertain.

Table 4. Fits to viscosity data of the form: log η= A +B/(*T*-C)

Sample	A	B(K)	C(K)	T_{12}(K)	number	RMS error	fragility[a]
1895	-4.69	5998.5	446.7	806	9	0.02	37.4
1926	-4.44	5999.5	477.5	842	10	0.04	38.0
1960	-4.51	5998.4	445.2	809	11	0.04	36.7
Vase	-4.37	5999.5	449.0	815	11	0.05	36.4
Haplogranite	-1.87	9001	494.4	1143	26	0.02	24.4
Leucogranite[b]	-6.98	18000	145.0	1093	36	0.02	21.9
Rhyolite	-4.65	12600	313.4	1070	22	0.08	23.5
Al-rhyolite	-7.30	17388	212.2	1113	27	0.05	23.8
Moldavite	-3.08	8997	488.5	1085	12	0.03	27.4
Indochinite	-3.16	8042	493.5	1024	36	0.03	29.3

Notes: The RMS error pertains to the fitting. Coefficient A has no units but is based on log (Pa s) per convention. Coefficient B has a similar basis. The last digit in the fitting parameters is uncertain.

[a] Calculated from the TVF parameters according $m = B/(T_{12}[1 - C/T_{12}]^2)$

[b] Data and TVF fit from Whittington et al. (2009b)

Table 5. Thermal diffusivity values and fitting parameters for glasses.

Sample	Thickness	T	D_{298}	$D = a + bT^{-1} + cT$				T_{max}[a]	$D = fT^{-0.4} + hT$		
	mm	°C	mm^2s^{-1}	a	b	c	R	(K)	f	h	R
1895	0.55[d]	25.3	0.55	0.428	34	0	0.98	900	4.90	1.66×10^{-4}	0.97
1960-1	0.91[d]	22.2	0.66	0.336	98	0	0.99	800			
1960-1 rerun	0.672	22.4	0.48								
1960-2 rerun	0.91	22.2	0.49	0.348	38	0	0.97	870	4.31	1.28×10^{-4}	0.98
Vase	0.576	19.9	0.50	0.382	33	0	0.98	850	4.38	1.62×10^{-4}	0.99
Modern	1.124[b,d]	24.8	0.50	0.400	29	0	0.98	900	4.45	1.65×10^{-4}	0.98
1884	0.467	20.1	0.50								
1890	0.51	21	0.53								
1926-2	0.951	24.8	0.50								
1926-3	0.848[d]	26.5	0.53	0.383	40	0	0.97	700	4.70	1.3×10^{-4}	0.96
1926-4	0.74	24.0	0.57	0.422	45	0	0.99	900	5.20	1.49×10^{-4}	0.99
Haplogranite	0.6-0.8[e]	20	0.70	0.440	69	0.62×10^{-4}	0.99	1300	6.27	1.73×10^{-4}	0.99
Leucogranite	0.772[d]	24.3	0.67	0.40	70	0.88×10^{-4}	0.99	1200	5.95	1.83×10^{-4}	0.96
Rhyolite	0.4-0.9[e]	21	0.63	0.44	51	0.54×10^{-4}	0.95	1250	5.73	1.82×10^{-4}	0.91
Al-Rhyolite	0.962	20.0	0.63	0.375	65	0.97×10^{-4}	0.99	1260	5.53	1.87×10^{-4}	0.99
Moldavite	0.84[d]	22.4	0.68	0.32	87	1.9×10^{-4}	0.97	1000	5.80	2.27×10^{-4}	0.94
Indochinite[c]	0.86[d]	22.7	0.64	0.31	82	1.6×10^{-4}	0.98	1100	5.52	1.99×10^{-4}	0.97

Notes: Uncertainty in D is 2%, from benchmarking. R is the linear correlation coefficient for the fits. The last digit of each fitting coefficient (a,b,c,f,g) is uncertain, except for leucogranite and rhyolite, where c is uncertain by 20%. Two fits are provided. Units of coefficient a are mm^2s^{-1}; units of b are mm^2Ks^{-1}; units of c and h are $mm^2s^{-1}K^{-1}$; units of f are $mm^2s^{-1}K^{0.4}$.

[a] T_{max} is the limit to which all these fits can be projected to.

[b] The room temperature values for modern glass were obtained using thinner pieces.

[c] Bubbles formed during the run.

[d] Sputter coated with Pt before applying graphite.

[e] Fit includes runs on multiple sections.

Table 6. High temperature thermal diffusivity values

Sample	T_{sat}	D_{sat}	T_{melt}	D_{melt}
	K	mm^2s^{-1}	K	mm^2s^{-1}
1895	750-930	0.47	1000-1200	0.38
1960-all			950-1200	0.32
Vase			950-1250	0.35
Modern			950-1300	0.36
1926-3	800-950	0.43	940-1170	0.35
1926-4			1000-1260	0.37[a]
Haplogranite	940-1320	0.57	1390-1650	0.54
Leucogranite			1320-1450	$0.47+0.36\times10^{-4}T$
Rhyolite	1100-1350	0.54	1350-1450	0.52
Al-rhyolite			1350-1550	$0.35+1.2\times10^{-4}T$
Moldavite			1250-1420	$0.35+1.6\times10^{-4}T$
Indochinite			1150-1310	$0.32+1.4\times10^{-4}T$

Notes: Uncertainties in *D* are 2% for the glass and 4% for the melt. Fits have linear correlation coefficients of 0.90 to 0.97

[a]The sample flowed during melting at high temperature, adding uncertainty to *D*-values.

Table 7. Volumetric thermal expansivity of glasses at 298 K and of melts at 1200 K, along with melt density

Sample	α_{glass} [a] $\times 10^{-6}$ K^{-1}	ρ_{melt} [b] kg m^{-3}	α_{melt} [b] $\times 10^{-6}$ K^{-1}	ρ_{melt} [c] kg m^{-3}	α_{melt} [c] $\times 10^{-6}$ K^{-1}
1895	29.4	2364	62.5	2370	61.5
1960	28.1	2390	62.8	2385	62.1
Vase	27.5	2400	58.3	2389	61.3
Modern	28.6	2411	62.2	2403	62.2
1926	27.2	2374	93.0	2393	57.2
Haplogranite				2308	24.62
Leucogranite				2327	24.54
Rhyolite				2326[d]	22.24[d]
Moldavite				2353	20.83
Indochinite				2426	24.47

Notes: Measured densities of the glasses are in Table 1. From comparing the two models, uncertainties are 2% for density and generally 5% for α_V.

[a]Thermal expansivity was calculated after Fluegel (2005) whose method is not geared to Al-rich melts. Results for 1884 and 1890 are similar to 1926 glass.

[b]Density of the melt was calculated after Flugel et al. (2008), whose method is not geared to Al-rich melts. Results for 1884 and 1890 are similar to 1926 and closely resemble measured $\rho(T)$ for Na-Ca melts.

[c]Calculated after Lange (1997) and Lange and Carmichael (1990).

[d]Al-rhyolite is assumed the same as rhyolite.

Table 8. Fits to thermal conductivity in $Wm^{-1}K^{-1}$

Sample	$k_{glass} = a + bT + cT^2 + dT^3$				$k_{melt} = a + bT$	
	a	b	$c\times10^6$	$d\times10^9$	a	$b\times10^4$
1895	0.669	0.00196	-1.95	0.70	1.39	-0.808
1960	0.647	0.00147	-1.51	0.55	1.23	-0.720
Vase	0.601	0.00180	-1.82	0.66	1.32	-0.721
Modern	0.572	0.00197	-1.97	0.71	1.38	-0.800
1926-3	0.695	0.00153	-1.52	0.55	1.35	-1.08
Haplogranite	0.734	0.00213	-2.15	0.80	1.74	-0.416
Leucogranite	0.737	0.00199	-1.92	0.72	1.52	0.753
Rhyolite	0.703	0.00202	-1.71	0.57	0.856[a]	5.18
Moldavite	0.795	0.00158	-1.26	0.49	0.980	6.15
Indochinite	0.792	0.00151	-1.28	0.51	1.12	4.41

Notes: The last digit of the fits are uncertain. Linear correlation coefficients are ~0.99. Units of coefficient a are $Wm^{-1}K^{-1}$; units of b are $Wm^{-1}K^{-2}$; units of c are $Wm^{-1}K^{-3}$; units of d are $Wm^{-1}K^{-4}$

[a]The fit for the melt is Al-rhyolite shifted to match the result upon melting for rhyolite.